THE UNIVERSITY OF MANITOBA

# OFFSET PARABOLOID ANTENNAS FOR MULTIPLE BEAM APPLICATIONS

BY

AHMED ASHRAF ZAGHLOUL

A THESIS

SUBMITTED TO THE FACULTY OF GRADUATE STUDIES

IN PARTIAL FULFILLMENT OF THE REQUIREMENTS FOR THE DEGREE

OF MASTER OF SCIENCE

DEPATRTMENT OF ELECTRICAL ENGINEERING

WINNIPEG, MANITOBA

September 1979

# OFFSET PARABOLOID ANTENNAS FOR MULTIPLE BEAM APPLICATIONS

BY

AHMED ASHRAF ZAGHLOUL

A thesis submitted to the Faculty of Graduate Studies of
the University of Manitoba in partial fulfillment of the requirements
of the degree of

MASTER OF SCIENCE

## ABSTRACT

The performance of offset reflector antennas with offset feeds is investigated. Mathematical expressions for the reflector pattern calculations by both the vector current and the scalar aperture methods are developed and are used to compute the co-polar and the cross-polar radiations. A computer program is prepared which utilizes a two dimensional integration to compute the required patterns for both methods. It is found that the scalar aperture method succeeds in predicting the co-polar pattern quite accurately. However, this method always predicts lower cross polarization level than those predicted by the vector current method. The computation time required by both methods for their pattern calculations is found to be comparable. It is also found that the gain of the reflector is not affected by small displacement in the feed. Shifting the feed along the reflector axis of symmetry is recommended since it has a negligible effect on the co-polar radiation and improves the cross-polar one.

ACKNOWLEDGEMENTS

The author wishes to express his appreciation to Dr. L. Shafai for his continuous interest, helpful advice, cheerful and able guidance in all phases of this work.

The financial assistance provided by the Communication Research Centre and the department of Electrical Engineering of the University of Manitoba are gratefully acknowledged.

TABLE OF CONTENTS

LIST OF FIGURES

# Chapter I

## INTRODUCTION

Recent developments in satellite and microwave communication systems as well as radio astronomical research have generated a great deal of interest in reflector type antennas. The reflector antennas are used with systems for communication or radar purposes in which a large value of gain, low side lobe level and low cross polarization are necessary.

At UHF frequencies and above, where pencil beams become practical, reflector antennas may be compared with other systems. The end fire or yagi antenna produces relatively high gain but suffers from a narrow frequency band. The phased arrays can be used to produce gain equal to those of reflector antennas, however, they are not universally useful, since they have complicated structures and are costly to produce. On the other hand, the reflector systems have simple geometries and are usually inexpensive to fabricate. They can also be serviced mechanically with far less sophistication than phased arrays. As a single monolithic unit on a mechanical scanning assembly, a reflector is relatively inexpensive to scan. A phased array, on the other

hand, requires a phase shifter for each element or at least for each subarray. Therefore, the reflecting systems are the appropriate choice for most point to point communication systems unless the system requires certain particular characteristics, such as a wide and continuous scanning, where the phased array is a better choice [1].

In reflecting systems, the reflectors are mainly used to modify the radiation from a radiating element or feed. The reflectors that are of most interest in the antenna field are all derived from conic sections; Their cross section can take the form of any of the five conic sections circle, ellipse, parabola, hyperbola and the straight line. The reflecting surfaces are normally generated by translation of the curves or by rotation around the focal axis to generate a surface of revolution. Such reflectors, provided that their surfaces are smooth, are truely wide band devices, capable in principle of operation from radio to optical frequencies.

In single reflector systems, the parabola is the most commonly used conic section, with a primary source located at the focus and directed into the reflector area. Since the reflector surface is fixed, the focal system must therefore be designed to give the desired radiation pattern. Also in most practical antennas the reflector aperture angle, from

the focus, is large and for a proper illumination its feed must have a wide angle radiation pattern. Because of its simplicity it has been studied exhaustively, but the description of all its properties is beyond the scope of this thesis. It is divided into two basic configurations, symmetric and offset. The symmetric configuration has been more popular and has been studied in more detail. With multiple off-axis feeds, it is also capable of producing multiple off-axis beams. However, this is at a cost of gain reduction.

The multiple reflector systems are also commonly used for their high magnification and short focal length. The Cassegrain antenna is the most common one among the multi-reflector systems. It consists of a main parabolic reflector and a secondary hyperbolic sub-reflector as shown in figure (1). The performance of the cassegrain system is affected by the blocking of the main aperture by the sub-reflector, the diffraction from the supporting structures and reflector edges and the spillover loss from the feed.

The use of reflectors as a microwave antenna started during the second world war with the invention of radar. The necessity to design useful systems stimulated a concentrated effort to develop a coherent and unified theory of reflector antennas founded on a solid base of physical

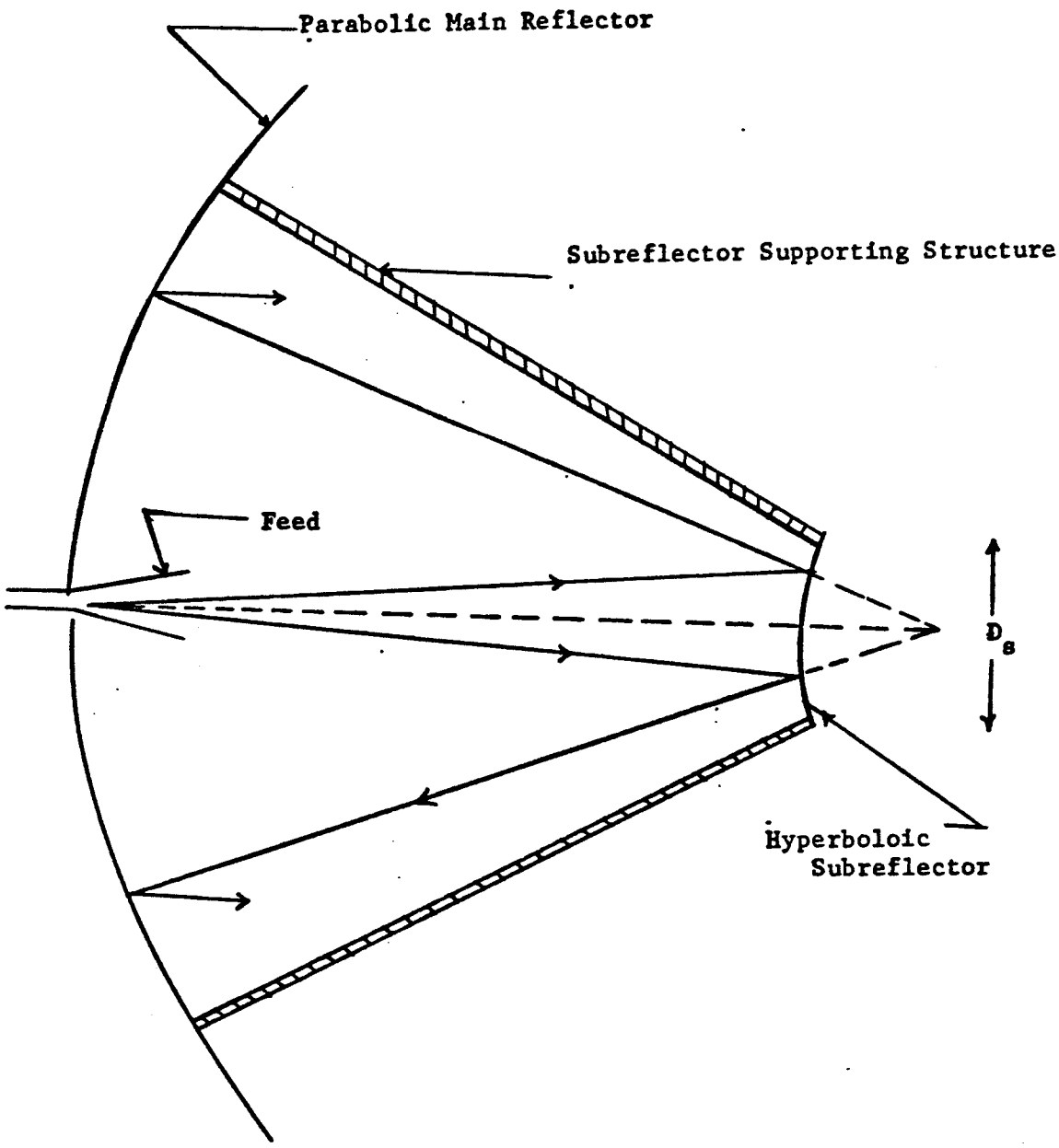


Figure 1. Classical Cassegrain Antenna.

electromagnetics theory. One of the first works published dealing with the polarization characteristics of reflector antennas was that of Cutler [2] who showed qualitatively that the ideal feed should radiate a spherical wave. He also examined the polarization characteristics of the then popular dipole feed and showed that it would give rise to cross polarization components in the reflected field.

The development of commmunication satellites and the arising need to track space probes during the sixties, demanded an increase in the aperture efficiency and a reduction in the feed spillover. The achievment of these goals was important since it would maximize the gain/temperature ratio (G/T) and reduce the cost. The reduction of the cost is essential since the cost of a single large reflector antenna is proportional to its diameter raised to the power 2.78 [3].

Galindo [4] showed that with a two reflector system it is possible to achieve arbitrary phase and amplitude distribution over the main aperture. Williams [5] described a modified cassegrain system, to which this approach was elegantly applied, leading to an improvement of about 2.5 % in the aperture efficiency.

By (1960) the horn had replaced the dipole as a reflector feed. But the characteristics of the horn's dominant mode were far from ideal for the purpose. This is mainly because its principle E and H plane radiation patterns are quite different. Potter [6] solved this problem in the case of the $TE_{11}$ mode excited conical horn. He showed that a correct combination of $TE_{11}$ and $TM_{11}$ modes (generated by a step discontinuity in the diameter near the throat of the horn) at the horn aperture would lead to a radiation pattern having almost identical patterns in the E and the H planes.

Ruze [7] has discussed the beam shift and the degradation of a paraboloidal reflector performance with an offset feed. He also presented the beam characteristics of a tapered circular symmetric illumination. His calculations were for small offsets in the feed with respect to the wave length which made it possible to apply the scalar aperture method. On the other hand, Imbrial et al [8] computed the radiation pattern of a parabolic reflector with large lateral feed displacments of a symmetric paraboloid. They utilized both the vector current method and the scalar aperture theory and compared their computed results with experiments. In particular, they showed that the gain computed by the scalar aperture method tends to deviate significantly from the experimental ones as the feed displacement increases. The vector current method, on the other hand, gives satisfactory results.

In recent years, the use of offset paraboloid reflectors has found wide application, especially in satellite communication, because of certain advantages they offer over their axi-symmetric full paraboloidal counterpart. Their use in the past has tended to be restricted to applications where electrical performance specifications have been severe. This is due to the fact that the offset geometry is more difficult to deal with and more costly to fabricate. However, from a theoretical point of view, their study is relatively more accurate. In axi-symmetric paraboloids, the blocking of the aperture by the feed and its supporting structures results in the reduction of the antenna gain, a general degradation in the suppresion of side lobes and across polarized radiation which generally limits the performance of the antenna. Aperture blockage also makes the theoretical investigation of the axi-symmetric paraboloid more complicated than that of the offset reflector. Furthermore, the computation of the aperture blockage can only be carried out approximately, and the computed performance of the reflector with an aperture blockage seldom agrees accurately with experimental data [9].

The offset system has the advantage of reducing the mutual reaction between the reflector and the primary feed. It also makes it possible to use a larger focal length to

diameter ratio while maintaining an acceptable structural rigidity. As a result, offset reflector primary feeds employ a larger radiating aperture, which in certain cases can improve the shaping of the primary pattern and give a better suppression of the cross polarized radiation emanating from the feed itself.

In many applications the structual pecularities of the offset reflector can be used to good advantage. For example, in the design of space craft antennas an offset configuration can often be accommodated more satisfactorily than an axi-symmetric design.

The initial work on the analysis of the offset reflector geometry was carried out by Cook et al [10] who were concerned with the analyses of a dual reflector open cassegrain system. The cross polarized radiation for linearly polarized excitation and the beam displacement for circularly polarized excitations have been investigated by Chu and Turrin [11]. They have given numerical calculations for the dependence of the radiation pattern upon the offset angle $\theta_0$ , as well as, the half angle of illumination $\theta_c$ . They also provided detailed graphical data and a clear insight into the beam squinting properties of the circularly polarized prime focus fed offset reflectors. These depolarizing and squinting phenomena are often

undesirable in high performance antennas, especially when frequency re-use is required. In many cases these effects constitute a major limitation in the application of an offset reflector, regardless of its other desirable properties.

Rudge [12] described two theoretical models for the prediction of the far field radiation from offset reflector antennas. The models can accommodate small offsets in the primary feed location, with respect to the reflector geometric focus and can thus be usefully employed in the study or design of multiple beam antennas. Experimental verification of the models has indicated that over a moderate range of angles about the antenna boresight, reliable predictions of the significant copolarized and cross polarized radiation can be obtained by the use of these methods. He has also shown that the maximum levels of reflector generated cross polarized radiation are comparatively insensitive to small offsets in the primary feed locations from the geometric focus.

A misunderstanding of the polarization properities of offset reflectors due to the belief that poor polarization is a property of the offset reflector, had put in the past restrictions on their application. Jacobsen [13] has shown that the reflector does not contribute to the cross

polarization in the far field. Neither is it a necessary consequence of the asymetry of the configuration. He has shown that the cross polarization of the far field is due to the cross polarization of the primary feed after collimation by the reflector. Therefore the cross polarization can be decreased by improving the feed.

A new class of improved primary feed called the matched feed has recently been introduced [14]. The design of this feed type can be best explained by studying the focal plane field of offset reflectors. In the reception mode, a linearly polarized and uniform plane wave incident along the axis of a parabolic metallic surface induces a surface current which in turn gives rise to a particular field distribution in the focal plane region of the reflector. By reciprocity, any primary feed that can synthesize the entire focal plane field distribution would, upon transmission, produce a linearly polarized and uniform plane wave field distribution in the projected aperture with 100% aperture efficiency. This is why the concept is known as the matched feed concept, since it identifies the focal fields as those corresponding to an optimum feed aperture field distribution , in the sense of achieving maximum aperture efficiency [15]. This concept has been utilized, with considerable success, in the development of high efficiency feeds for both axi-symmetric [16] as well as offset systems [17], [18].

Bem [17] studied the electric field distribution in the focal region of an offset paraboloid. He determined the current distribution on the reflecting surface from the boundary conditions when a uniform plane wave is incident on the reflector. He treated each surface element as an elementary dipole producing an elementary field at a point near the focus. The total field at the focus is obtained by integration over the whole reflecting surface. He carried out the integration for a long focal length.

The focal field in the plane of symmetry was found to be;

$$E_x = K' \left[ \frac{J_1(u)}{u} + j \frac{d \sin\theta}{4 f} \frac{J_2(u)}{u} \cos\phi \right] , \qquad (1)$$

$$E_y = K' \left[ -j \frac{d \sin\theta_0}{4 f} \frac{J_2(u)}{u} \sin\phi \right] \qquad (2)$$

where $u = \frac{k r}{4 f} ( 1 + \cos\theta_0 )$ and

$J_n(u)$ is the Bessel function of order n .

The solution for the wave polarization in the plane of asymmetry is similar to the above expressions, but is obtained by interchanging x and y and replacing $\phi$ with $(2\pi - \phi)$. That is ;

$$E_x = K' \left[ -j \frac{d \sin\theta_0}{4 f} \frac{J_2(u)}{u} \sin\phi \right] , \qquad (3)$$

$$E_y = K' \left[ \frac{J_1(u)}{u} + j \frac{d \sin\theta_0}{4f} \frac{J_2(u)}{u} \cos\phi \right] \qquad (4)$$

An inspection of the above two cases shows that the cross-polar component is an asymmetrical function of $\phi$ with a magnitude which decreases with the decrease of the offset angle . The focal plane field is shown in figure (2) as a superposition of two configurations of the symmetric and the antisymmetric field distributions of two polarizations. For the primary feed to provide a match to these incoming fields, its aperture must exhibit similar linear polarization properties. It is a fact that conventional high performance axisymmetric feeds provide an excellent match to only the co-polar component, which leads to poor cross-polar radiation characteristics of the antenna. Rudge et al [14] explained how the symmetric component can be well matched by making use of higher order asymmetrical wave guide modes.

The matched feed used in this thesis is the same one designed by Aboul-Atta and Shafai [15]. They have shown that the improved class of primary feed devices must be at least bimodal in the sense of radiating a fundamental $TE_{11}$ mode plus a compensating $TE_{21}$ mode. The necessary condition is that these two modes be in phase quadrature at the aperture of the device. Since the compensating mode has a skew-symmetric field distribution in the aperture then upon radiation, its generated field becomes in phase with the

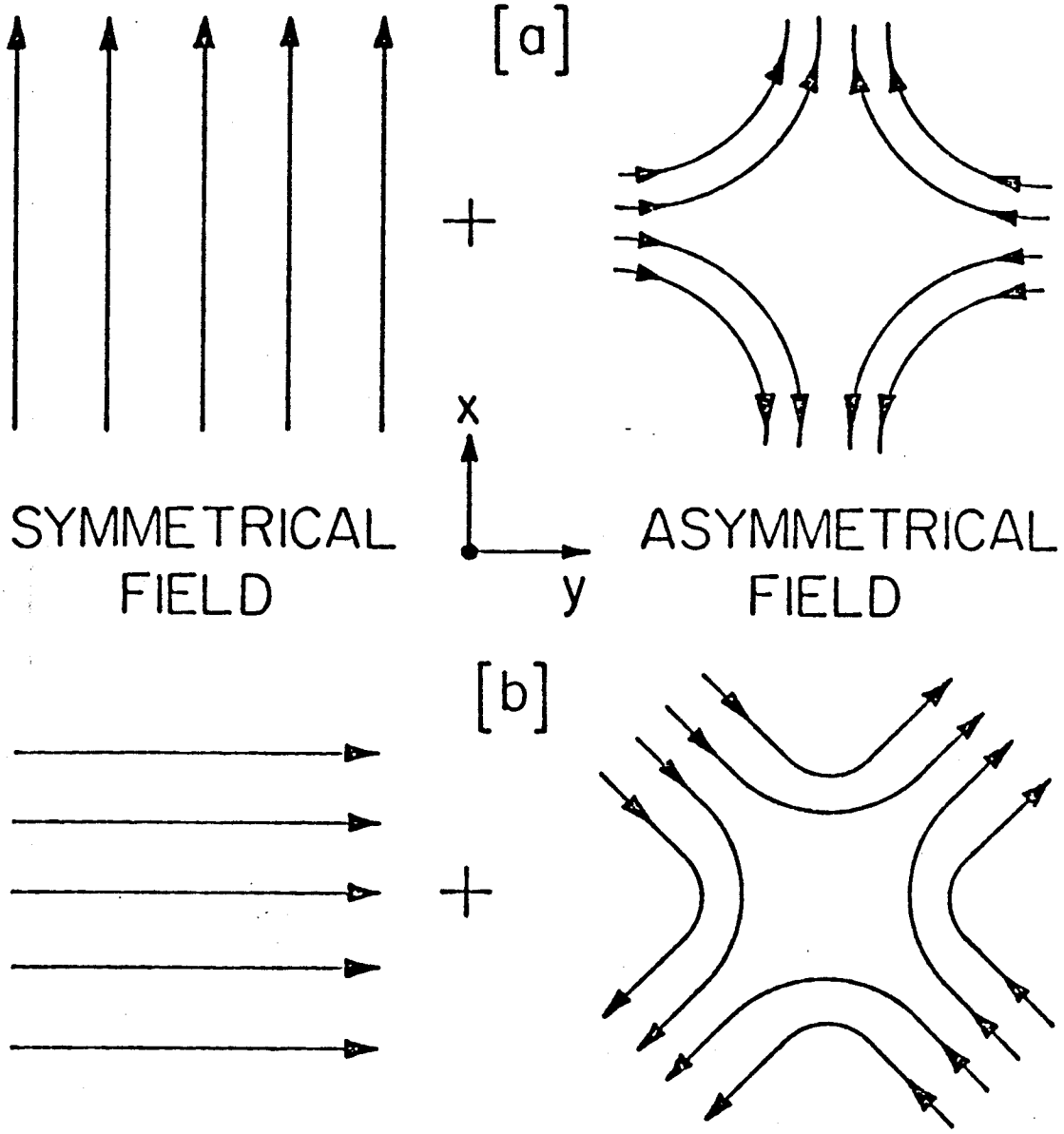


Fig. 2 Symmetric and asymmetric components of the offset reflector focal-plane field.
[a] Polarization in the plane of symmetry.
[b] Polarization in the plane of asymmetry.

fundamental radiation. Hence the total radiation field from a matched feed device at a distance R, may be expressed by [15]

$$E_T = [\, E^{(1)} + E^{(2)} \,] \quad \frac{\exp(-jkR)}{R} \tag{5}$$

where $E^{(1)}$ and $E^{(2)}$ are real quantities representing the angular variation $(\theta, \phi)$ of the respective radiation of the fundamental and the compensating modes.

$E^{(1)}(\theta)$ and $H^{(1)}(\theta)$ describe the E and the H plane radiation pattern functions of the fundamental mode and for $TE_{11}$ circular waveguide mode are given by

$$E^{(1)}(\theta) = (1 + \cos\theta) \frac{J_1(u)}{u} , \tag{6}$$

$$H^{(1)}(\theta) = (1 + \cos\theta) \frac{J_1'(u)}{1 - \left(\frac{u}{p_{11}}\right)^2} \tag{7}$$

where $J_n(u)$ is the Bessel function of order n ,

$p_{mn}$ is the $n^{th}$ root of $J_m(u)$ ,

$$u = \frac{d'}{\lambda} \sin\theta$$

with $d'$ is the diameter of the primary feed aperture.

For the compensating $TE_{21}$ mode the functions take the form

$$E^{(2)}(\theta) = \alpha\,(1+\cos\theta)\,\frac{2J_2(u)}{u}\,, \tag{8}$$

$$H^{(2)}(\theta) = \alpha\,(1+\cos\theta)\,\frac{J_2'(u)}{\left(1-\left(\frac{u}{p_{21}}\right)^2\right)} \tag{9}$$

where $\alpha$ is the ratio between the $TE_{11}$ and the $TE_{21}$ modes. Equation (5) represents the new primary feed radiation that is to be used in the calculation of the performance of the antenna.

It should be noticed that the relative amplitude of the compensating mode is dependent upon the parameters of the reflector. These parameters are the offset angle $\theta_0$ and f/d ratio of the reflector.

Aboul-Atta and Shafai [15] gave two examples to show the advantages of this type of feed and the effect of the reflector parameters on its performance. The first example was a reflector with $50^0$ offset angle and f/d=0.4773 (aperture angle=$45^0$ , D=100$\lambda$). The original -17 dB cross-polar radiation of the reflector without $TE_{11}$ mode, was reduced to less than -36 db after adding a $TE_{21}$ mode with 0.3 mixing ratio. However, the overall antenna efficiency was dropped from 63.12 % to 62.18 % . This was due to the fact that the above aperture angle was no longer the optimum angle after adding the $TE_{21}$ mode which modifies the feed

pattern. The efficiency was then increased to 65.597 % by increasing the aperture angle from $45^0$ to $50^0$.

The second example showed the radiation pattern of a reflector with an offset angle of $30^0$ and f/d=0.833. The required mixing ratio $\alpha$ was 0.07 which was much smaller than that of the previous case. It was found that the cross-polar radiation dropped to around -50 db of the co-polar field. In addition the antenna efficiency was found to be much larger.

From the above two examples, they have recomended that the geometry of the reflector be selected to have small offset angles and large f/d ratios. This geometry will yield a high antenna efficiency and will require a smaller mixing ratio . The small mixing ratios require smaller obstacles in the waveguide to generate the compensating mode, which improves its frequency performance and simplifies its design.

It should be noted that this method for the design of the feed is more accurate than that given by Bem [17]. Bem's expression is based on a series expansion and to increase its accuracy more terms have to be taken into account, that is to say more modes have to be generated which will complicate the design of the feed and will narrow its frequency bandwidth.

This thesis considers the offset reflector antennas for multiple beam applications, mainly for Canadian satellite use. Assuming a geostationary orbit, the communication needs of major Canadian cities may be accomodated by using only several narrow beams. From a central geostationary orbit, all Canadian cities can be seen by off axis beams clustered within $\pm 4^0$ . We are therefore interested in the performance of offset systems capable of generating off axis beams within $\pm 4^0$, and with adequate polarization isolation. To allow for a possible off centre satellite location, beam shifts as large as $\pm 5^0$ will be considered.

In chapter two, the geometry of offset reflectors is defined in detail, and the different definitions of cross polarization are discussed. In chapter three, mathematical expressions necessary for reflector pattern calculations are developed for both the current distribution and the aperture field methods. In chapter four, the radiation patterns of offset reflectors with offset feeds are investigated by both the vector current and the scalar aperture methods. The computed patterns by the vector current method and a comparison of the two methods is presented in chapter five.

## Chapter II

## IMPORTANT DEFINITIONS ASSOCIATED WITH OFFSET SYSTEMS

### 2.1 INTRODUCTION

There is an ambiguity associated with the word offset as it is currently used in antenna engineering. One meaning refers to the reflector, an offset paraboloid is taken to be one which is not symmetrical about its axis of revolution. The portion of the reflector surface lying on one side of that axis is discarded altogether. Since the feed must still be located on or very close to the axis, this arrangement removes the feed from the region of highest aperture field intensity and reduces or may even eliminates blockage. Of course the axis of the feed is tilted so that its cone of illumination will be on that part of the reflector surface that remains. Otherwise, the spillover will be excessive. The other meaning associated with offset is one in which the phase centre of the feed is displaced laterally from the optical axis in order to squint the beam.

As there is an ambiguity associated with the word offset, there is also a lack of precise and unambiguous definition of cross polarization. The whole subject of cross polarization in reflector antennas had been somewhat con-

fused for many years and had given rise to certain misunderstanding and controversies. Ludwig points out in his paper [19] this surprising deficiency and attempts to correct it. He discusses three different definitions that are commonly used. He then shows where they are applicable and how they differ.

In this chapter the two meanings associated with the word offset are clarfied and the offset reflector geometry is discussed in detail. The reflector's various parameters are defined and equations describing its surface for both spherical and rectangular coordinates are given. Also different definitions of cross polarization are discussed. Ludwig's third definition is used in this thesis for the predicted field components. This definition corresponds directly to the components measured using standard antenna range techniques.

## 2.2 OFFSET REFLECTOR GEOMETRY

An offset paraboloid is taken to be one which is not symmetrical about its axis of revolution. The geometry of an offset reflector is shown in figure (3). The basic parameters of the reflector are f, $\theta_0$ and $\theta_c$ where f is the focal length of the parent paraboloid, $\theta_0$ is the offset angle and $\theta_c$ , the half angle of illumination, is the half angle subtended at the focus by any point at the reflector rim.

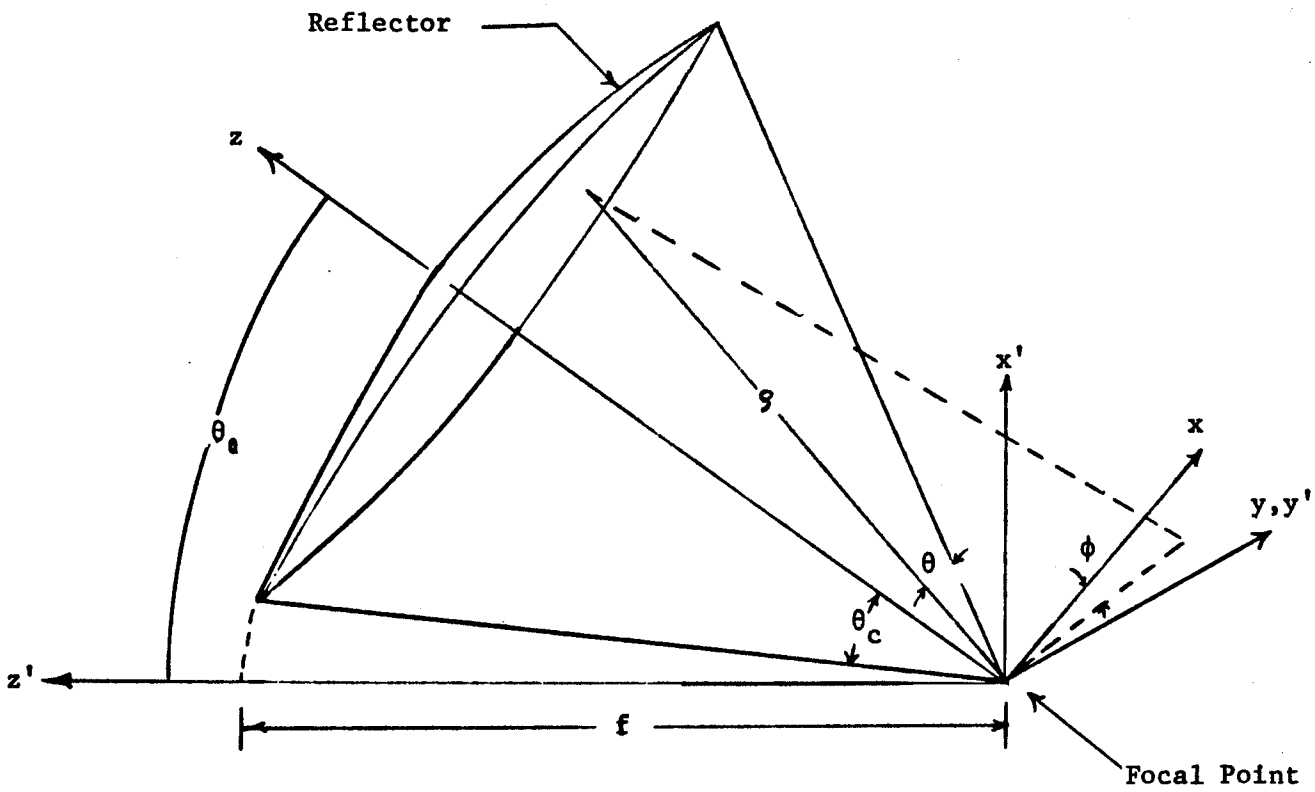


Figure 3. Offset Reflector Coordinate System.

Ingerson and Wong [20] defined an offset axis as the line through the focus that bisects the angle subtended at the focal point by the parabolic arc of the reflector in its plane of symmetry. It follows that the offset focal plane is the plane through the focus and perpendicular to the offset axis. With these definitions, the focal region characteristics of offset reflectors are quite analogus to those of symmetrical reflectors.

The offset reflector may be defined in two coordinate systems; $x',y',z'$ which defines the parent paraboloid and the rotated system $x,y,z/\ \rho, \theta, \phi$ which is more convenient in describing the radiation pattern of a feed located at the reflector focus. The transformation from one system to another and the equation of the reflector in various coordinate systems are given in Appendix (A).

The physical contour of the reflector is elliptical but its projection onto the xy plane produces a true circle.

The parameters that are of interest in this work are :

The diameter d of the projected aperture

$$d = \frac{4\ f\ \sin\theta_c}{\cos\theta_0 + \cos\theta_c} \qquad (10)$$

The differential surface element ds

$$ds = \frac{dx'\ dy'}{\cos\theta'/2} = \frac{r^2 \sin\theta\ d\theta\ d\phi}{\cos\theta'/2} \qquad (11)$$

And the distance r from the reflector focus to a point on a parabolic surface

$$r = \frac{2f}{1 + \cos\theta'} \qquad (12)$$

or

$$r = \frac{2f}{1 + \cos\theta\cos\theta_0 - \sin\theta\sin\theta_0\cos\phi} \,. \qquad (13)$$

For any surface represented by a radius vector, the unit normal is given by : [17]

$$\bar{n} = \frac{-\bar{r}_\theta \times \bar{r}_\phi}{|\bar{r}_\theta \times \bar{r}_\phi|} \qquad (14)$$

where

$$\bar{r}_\theta = \frac{d\bar{r}}{d\theta} \quad \text{and} \quad \bar{r}_\phi = \frac{d\bar{r}}{d\phi} \,.$$

In the rectangular coordinate system this may be given by

$$\bar{n} = n_x \bar{x} + n_y \bar{y} + n_z \bar{z} \qquad (15)$$

where

$$n_x = -\left(\frac{r}{4f}\right)^{\frac{1}{2}} (\sin\theta\cos\phi - \sin\theta_0) ,$$

$$n_y = -\left(\frac{r}{4f}\right)^{\frac{1}{2}} \sin\theta\sin\phi , \qquad (16)$$

$$n_z = -\left(\frac{r}{4f}\right)^{\frac{1}{2}} (\cos\theta + \cos\theta_0) ,$$

$\bar{x},\bar{y},\bar{z}$ are the unit vectors of the x,y,z coordinate system .

The diameter of the parent paraboloid D is given by

$$D = 4f \tan\left(\frac{\theta_0 + \theta_c}{2}\right) \qquad (17)$$

while the distance $X_0$ from the axis of the parent paraboloid to the centre of the projected aperture is

$$X_0 = \frac{2f\sin\theta_0}{\cos\theta_0 + \cos\theta_c} . \qquad (18)$$

## 2.3 THE DEFINITION OF CROSS POLARIZATION

The possible use of orthogonal polarization to provide two communication channels for each frequency to save frequency bandwidth has led to interest in the polarization purity of antenna patterns. However, there is no universaly accepted definition of the cross polarization at present. According to IEEE standard definitions [20], the co-polarization and the cross-polarization is defined by comparing the source with a reference source. The co-polar field of the given source is then taken to be the component of the field which is parallel to the field of the reference source and the cross-polar field is the orthogonal component. This means that the co-polar field of a given source is defined by

$$\overline{E}_{co} = \frac{\overline{E} \cdot \overline{E}_{ref}}{E_{ref}^2} \overline{E}_{ref} \qquad (19)$$

where $\overline{E}$ is the electric vector field of a given source and $\overline{E}_{ref}$ is the electric vector field of the reference source.

Ludwig discussed three different definitions of the cross polarization in his 1973 paper [19]. He designated them as first, second, and third definitions according to the reference field being: 1) a plane wave, 2) the radiated E-field from a short electric dipole, 3) the E-field radiated by a Huygens source.

The definition used in this thesis is the third definition. With this choice, the principally polarized or co-polar field is that which would be measured by a conventional antenna range technique with the polarization of the distant source initially aligned with that of the test antenna on boresight and remaining fixed while the test antenna is rotated in the normal way to produce the measured radiation pattern. If the polarization of the distant source antenna is then rotated 90 degrees and the radiation pattern measurement repeated , the produced data represents a measurement of the cross-polar field components [21]. This definition has the advantage that the predicted field component at any point in space, corresponds to the components measured using a standard antenna range technique [22]. Employing this definition, the co-polar and cross-polar radiations for a linearly polarized feed are

$$\begin{bmatrix} E_p \\ E_q \end{bmatrix} = \begin{bmatrix} -\sin\phi & \cos\phi \\ \cos\Phi & \sin\phi \end{bmatrix} \begin{bmatrix} E_\Psi \\ E_\Phi \end{bmatrix} \qquad (20)$$

Where $E_p$ & $E_q$ are the co-polar and the cross-polar radiation fields, respectively, and $E_\Psi$ & $E_\Phi$ are the radiation fields of the reflector in the conventional spherical coordinate system $(r,\Psi,\Phi)$ with origin at the focus of the reflector.

# Chapter III

# FORMULATION OF FIELD OF REFLECTORS

## 3.1 INTRODUCTION

Exact solutions of the scattering problem have been obtained for only a limited number of cases involving simple primary fields and reflectors of simple geometry, such as spheres and cylinders. In treating reflectors of arbitary shape it is necessary to resort to approximate techniques. Two such techniques are discussed in detail in this chapter. The first method is the current distribution method. In this method an integral equation is formulated which contains the induced current distribution on the antenna or scatterer as the unknown quantity. Once the current distribution is obtained, all the important characteristic properties (scattering or radiation pattern) may be easily determined.

The second method is the aperture field method. This method determines the distribution of the tangential electric field on the focal plane projected aperture. This has the advantage of leading to simpler mathematical expressions, and is prefered over the current distribution method, since, within a 30 degree cone angle, it predicts a far field radiation pattern close to that of the surface cur-

rent method. However, a similar simple expression for the radiation pattern for the current distribution method is derived in the next section.

The radiation can also be calculated by applying the geometrical theory of diffraction (GTD). The GTD is an approximate asymptotic method which treats diffraction as a localized phenomena, and allows one to obtain the scattered field directly from purely geometrical considerations. Using simple ray tracing, one can include contributions to the scattered field due to geometrical optics reflection, as well as the diffraction fields from edges and corners.

Since the GTD is an asymtotic method, it is expected to give more accurate results as the frequency of excitation is increased. In contrast with the first two methods, the GTD method works best for larger bodies. Tsai [23] in comparing between the integral equation method and the GTD showed that integral equation methods are more accurate for small structures, are applicable to a wide range of geometric configurations, and provide more information (current,impedence,...etc). On the other hand the GTD method is accurate for large structures and is easily adaptable for a change in the polarization.

## 3.2 THE CURRENT DISTRIBUTION METHOD

The current distribution method discussed in this section has the advantage of leading to a good approximation for the scattered field and also makes it possible to analyse secondary effects such as the reaction of the reflector on the surface.

The main feature of this method is that it approximates the current distribution over the surface of the reflector. The scattered field is obtained from the current distribution using the following equations [22] :

$$E = \frac{-j}{4\pi\omega\varepsilon} \int_s [ ( \bar{K} \cdot \nabla ) \nabla + k^2 \bar{K} ] \frac{\exp(-jkr)}{r} ds, \qquad (21)$$

$$H = \frac{1}{4\pi} \int_s ( \bar{K} \times \nabla ) \frac{\exp(-jkr)}{r} ds \qquad (22)$$

where r is the distance from the field point to the element of the surface ds .

The current distribution over the reflector is obtained on the basis of geometrical optics, which yields good results only if the reflector surface is smooth and its

diameter is generally large with respect to the wavelength. This method assumes that there is no current over the shadow area of the reflector. The current distribution over the illuminated region is obtained on the assumption that at every point the incident field is reflected as though an infinite plane wave were incident on the finite tangent plane.

Silver [22] has shown that the scattered field intensity in the far zone is given by

$$E_s = \frac{-j\omega\mu \exp(-jkR)}{2\pi R} \int_s \{ \bar{n} \times \bar{H}_i - [ ( \bar{n} \times \bar{H}_i ) \cdot \bar{R}_1 ] \bar{R}_1 \} \cdot \exp(jk\bar{\rho} \cdot \bar{R}_1) \, ds \cdot \quad (23)$$

The magnetic field can be calculated from the far zone relation

$$H_s = \left(\frac{\varepsilon}{\mu}\right)^{\frac{1}{2}} ( \bar{R}_1 \times \bar{E}_s ) \quad (24)$$

where $\bar{\rho}$ is a vector from a given origin to the element of the surface ds , $R_1$ is a unit vector from the origin to the field point , the distance between them being R, n is a unit normal vector off the reflector and $H_i$ is the radiation field of the feed located at the focal point of the reflector.

As $H_i$ has no component in the $R_1$ direction, equation (23) reduces to

$$E_s = \frac{-j\,\omega\mu\,\exp(-jkR)}{2\,\pi\,R} \int_s (\bar{n} \times \bar{H}_i)\,\exp(jk\bar{\rho}\cdot\bar{R}_i)\,ds \quad (25)$$

Let $\bar{R}_1, \bar{i}_\Psi, \bar{i}_\Phi$ be unit vectors associated with the spherical coordinates $R, \Psi, \Phi$, then the radiation field of the reflector will be

$$E_\Psi = \frac{-j\,\omega\mu\,\exp(-jkR)}{2\,\pi\,R} \int_s (\bar{n} \times \bar{H}_i) \cdot \bar{i}_\Psi\,\exp(jk\bar{\rho}\cdot\bar{R}_1)\,ds, \quad (26)$$

$$E_\Phi = \frac{-j\,\omega\mu\,\exp(-jkR)}{2\,\pi R} \int_s (\bar{n} \times \bar{H}_i) \cdot \bar{i}_\Phi\,\exp(jk\bar{\rho}\cdot\bar{R}_1)\,ds \quad (27)$$

where $ds = \dfrac{r^2 \sin\theta}{\cos\frac{\theta'}{2}}\,d\theta\,d\phi$

Neglecting the z component for the far field region and for $\Psi$ around 180 degrees equations (26) and (27) reduce to

$$\begin{bmatrix} E_\Psi \\ E_\Phi \end{bmatrix} = \frac{-j\,\omega\mu\,\exp(-jkR)}{2\,\pi\,R} \begin{bmatrix} \cos\Psi\cos\Phi & \cos\Psi\sin\Phi \\ -\sin\Phi & \cos\Phi \end{bmatrix} \begin{bmatrix} I_x \\ I_y \end{bmatrix} \quad (28)$$

where

$$I_L = \int_0^{\theta_c} \int_0^{2\pi} \bar{L}.(\bar{n} \times \bar{H}_i) \exp[-jk(r-\bar{\rho}.\bar{R}_i)] \frac{r^2 \sin\theta}{\cos\frac{\theta'}{2}} d\theta\, d\phi \qquad (29)$$

with $\bar{L}$ being either $\bar{x}'$ or $\bar{y}'$

$$\text{and} \quad \bar{H}_i = ( A_\theta \bar{i}_\theta + A_\phi \bar{i}_\phi ) \frac{1}{r} . \qquad (30)$$

Applying the definition of the co-polar and the cross-polar components as defined in equation (20) we get

$$\begin{bmatrix} E_p \\ E_q \end{bmatrix} = \frac{-j\,\omega\mu \exp(-jkR)}{2\,\pi\,R} \cdot \begin{bmatrix} -(1+\cos\Psi)\sin\Phi\cos\Phi & -\cos\Psi \sin^2\Phi + \cos^2\Phi \\ \cos\Psi\cos^2\Phi - \sin^2\Phi & (1+\cos\Psi)\sin\Phi\cos\Phi \end{bmatrix} \begin{bmatrix} I_x \\ I_y \end{bmatrix} . \qquad (31)$$

Equation (31) is used for the computation of the co-polar pattern $E_p$ and the cross-polar pattern $E_q$.

## 3.3 THE APERTURE FIELD METHOD

This method has no special advantage over the current distribution method presented in the previous section for the treatment of an arbitrary reflector. However, it is preferable in the case of a paraboloidal reflector, since within a 30 degree cone angle, it predicts the far field radiation pattern with no significant difference with the calculated results of the current distribution method. It also leads to simpler mathematical expressions, and offers some reduction in the required computation effort.

The reflectors to which this method is particularly suited have the property that the entire family of rays reflected from the illuminated area $S_0$ lie in one hemisphere of space. Also in the neighborhood of the reflector it is possible to draw a finite curve $\Gamma_A$ circumscribing the entire family of the reflected rays as shown in figure(4). The shadow boundary $\Gamma$ on the reflector defines an aperture which can be regarded as arising from a distribution of image sources behind the reflector. The offset paraboloid antenna has this property and the aperture in this case is a circle.

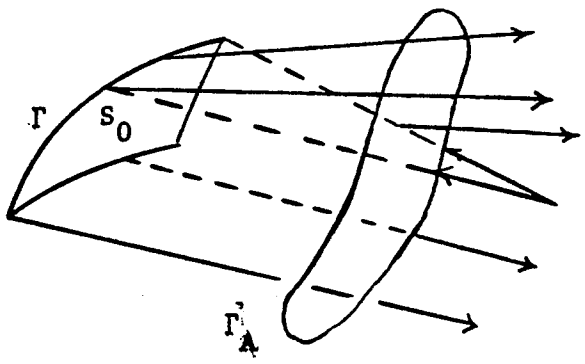


Figure 4. On The Aperture Field Method.

To utilize this method one needs the tangential electric field on the focal plane projected aperture region. The mathematical expression for the antenna vector radiation pattern has been given by Silver [22] ;

$$E_s(P) = \frac{-j\,k\,\exp(-jkR)}{4\,\pi\,R} \int_A \{ \bar{R}_1 \times [ ( \bar{R}_1 + \bar{n} ) \times \bar{E}_r ] \} \cdot \exp(jk\bar{\rho}\cdot\bar{R}_1)\, dA \quad (32)$$

where $\bar{R}_1$ , $\bar{n}$, $\bar{\rho}$ are the same as for the current distribution case, and $\bar{E}_r$ is the electric field reflected from the offset reflector and is obtained from [22]

$$\bar{E}_r = 2\,(\bar{n}\cdot\bar{E}_i)\,\bar{n} - \bar{E}_i \quad (33)$$

where $\bar{E}_i$ is the incident electric field at the reflector surface. Using the expressions given by Rudge [12], the normalized radiation pattern of the offset antenna is

$$\begin{bmatrix} E_{pn} \\ E_{qn} \end{bmatrix} = \frac{1+\cos\Psi}{2\,F_p(0,0)} \begin{bmatrix} 1 - t^2\cos 2\Phi & t^2 \sin 2\Phi \\ t^2 \sin 2\Phi & 1 + t^2 \cos 2\Phi \end{bmatrix} \begin{bmatrix} F_p(\Psi,\Phi) \\ F_q(\Psi,\Phi) \end{bmatrix} \quad (34)$$

where $E_{pn}$ is the co-polar component, $E_{qn}$ is the cross-polar component, $R,\Psi,\Phi$ are the field point coordinates, $F_p$ , $F_q$ are

the spatial fourier transforms of the co-polar and the cross-polar components of the electric field in the aperture plane and

$$t = \tan \frac{\Psi}{2}$$

The fourier transform integral is given by

$$F_i(\Psi,\Phi) = \int_0^{\theta_c} \int_0^{2\pi} \varepsilon_i \exp[\, -jk \, ( \, r - \bar{\rho} \cdot \bar{R}_1 \, ) \, ] \, r^2 \sin\theta \; d\theta \; d\phi \qquad (35)$$

where i is p or q ,

$$r = \frac{2 f}{( \, 1 + \cos\theta \cos\theta_0 - \sin\theta \, \sin\theta_0 \cos\phi \, )} \; ,$$

and

$$\begin{bmatrix} \varepsilon_p \\ \varepsilon_q \end{bmatrix} = K \begin{bmatrix} s_1 & -c_1 \\ c_1 & s_1 \end{bmatrix} \begin{bmatrix} A_\theta \\ A_\phi \end{bmatrix} \qquad (36)$$

where

$$s_1 = \sin\phi \, ( \, \cos\theta + \cos\theta_0 \, )$$

$$c_1 = \sin\theta \sin\theta_0 - \cos\phi \, ( \, 1 + \cos\theta \cos\theta_0 \, )$$

and $A_\theta$ and $A_\phi$ are defined from the incident field

$$\bar{E}_i = \frac{\exp(-jkr)}{r} \, ( \, A_\theta \, \bar{i}_\theta + A_\phi \, \bar{i}_\phi \, ) \; . \qquad (37)$$

# Chapter IV

# MULTIPLE BEAM ANTENNAS AND THEIR APPLICATIONS

## 4.1 INTRODUCTION

In many countries such as Canada and Japan, the communication needs of major cities may be accomodated by using several narrow beams. For example, from a geostationary orbit, the Canadian cities can be seen by off-axis beams contained within $\pm 4^{0}$ . This has led to a great deal of interest in multiple beam antennas.

To achieve a multiple beam system, it is required that the antenna s directional pattern be steerable over certain angles. This can be accomplished either by mechanically steering the reflector structure or by small displacements of the feed. Steering the reflector structure is not practical, especially for large antennas where the antenna and the associated backing structure may have a dead weight of the order of hundreds of tons and thus the steering requirement constitute a major part of the antenna systems. On the other hand, the displacement of the feed may involve the movement of a complex feed assembly. However, this compares favourably when considering the problems involved in moving the massive reflector structure. When a feed in a reflector

antenna is moved away from the focus in the transverse plane, the beam is displaced in the opposite direction and the beam is said to be scanned.

The performance of an axi-symmetric paraboloid with offset feed has been studied in detail. Ruze [7] studied lateral feed displacements in a paraboloid applying the scalar aperture method. He presented the properties of the offset fed paraboloids in the form of graphs of the significant characteristics. Later Imbriale et al [8] studied the same problem applying both the current distribution method and the scalar aperture method and compared the results of both methods with experimental ones.

Rudge [12] described two theoretical models for the prediction of the far field radiation from offset paraboloid antennas with offset feeds applying the scalar aperture technique. However, those models can only accommodate small offsets in the primary feed with respect to the reflector geometric focus. To the best of my knowledge, the problem of offset reflectors with large offset feed displacements and the accuracy of the scalar method as the displacement of the feed increases, has not been previously studied .

In this chapter, radiation patterns of offset reflectors with offset feed are investigated using two methods. The first method is the scalar aperture method, assuming that for small offsets of the feed, the radiation field may be considered stationary with respect to the reflector. This only adds a compensation term to the phase expression which accounts for small offsets in the primary feed.

The second method is the vector current method. This method no longer assumes that the field of the primary feed is stationry with respect to the reflector. Therefore, it is more accurate than the scalar method and is applicable to both small and large displacements in the feed.

## 4.2 THE SCALAR APERTURE METHOD

Offset paraboloid reflectors with offset feeds are used in satellite communication to achieve multiple beams. The feed displacement could be either transverse in the focal plane or longitudinal along the z axis as shown in figure (5), each able to achieve certain desired characteristics.

This method is based on the assumption that the magnitude of the primary field is equal to its value when the feed was located at the focus. It is an approximate method and is

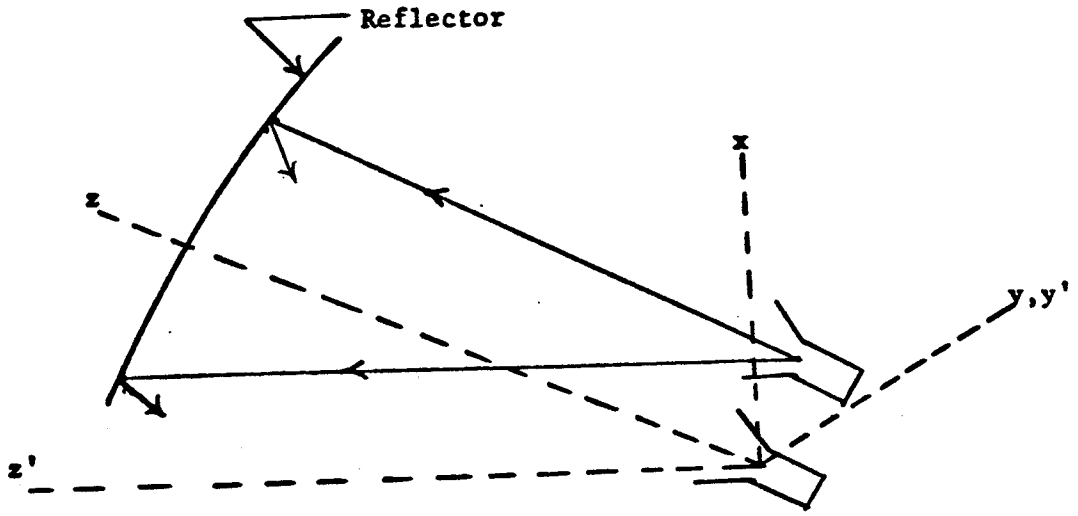


(a)

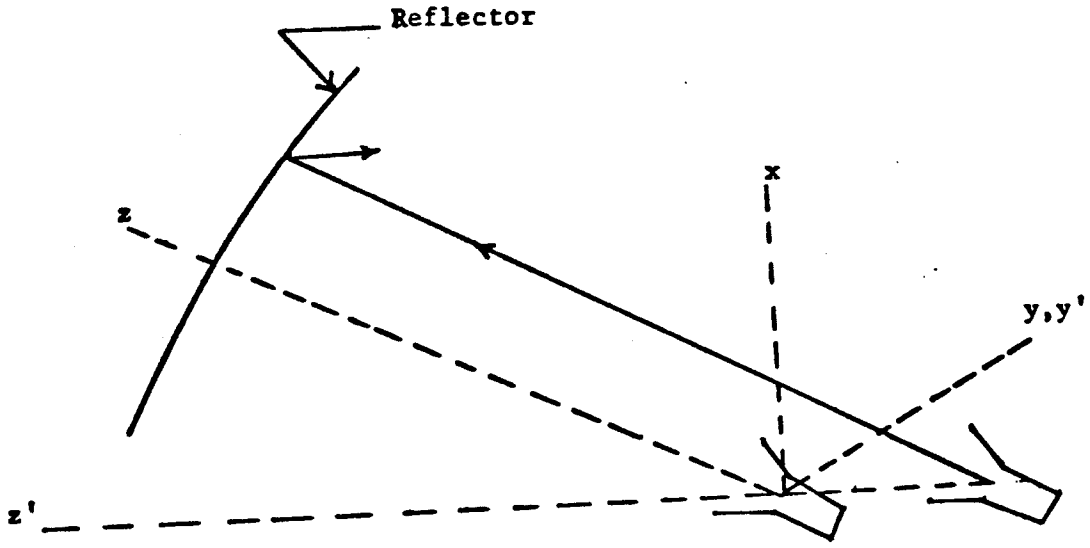


(b)

Figure 5. The Feed Displacement

a. Transverse in The Focal Plane

b. Longitudinal Along The z Axis

only applicable to the cases where the offset in the primary feed location from the geometric focus is small. This is due to the fact that the effect of the offset on the overall antenna radiation pattern is assumed to be negligable, which is only true for small offsets as the magnitude of the primary field is assumed to be fixed with respect to the reflector. Thus we only need to adjust the phase term which is very sensitive to any small displacement in the feed.

The adjustment of the phase expression of the feed is done by adding a compensation term that accounts for small offsets in the primary feed location. Thus equation (37) representing the primary feed before displacement becomes ;

$$\overline{E}_i = \frac{1}{r} \left(A_\theta \, \overline{i}_\theta + A_\phi \, \overline{i}_\phi \right) \exp[\, jk \, ( \, S - r \, )] \qquad (38)$$

where S is the compensating term. It is derived in Appendix (B) by the same procedure used by Ruze in his paper [5] and S is found to be

$$S = \varepsilon_t \sin\theta \, \cos( \, \phi - \phi_0 \, ) + \varepsilon_z \cos\theta \qquad (39)$$

where $\varepsilon_t$ is the transversal displacement and $\varepsilon_z$ is the axial displacement. It should be noted that $\varepsilon_t/r$ and $\varepsilon_z/r$ were assumed to be much less than unity in deriving S .

Now that the function S is known, we can substitute equation (38), describing the primary field after displacement, in equation (31) to calculate the radiation pattern by the current distribution method, or in equation (34) to calculate the pattern by the aperture field method. The resultant phase term in both equations will be the same and is equal to $r - \bar{\rho} \cdot \bar{R}_1 - S$ .

This phase term is simplified in Appendix (B) by assuming that the variation of $\cos\Psi$ can be neglected in the region about $\Psi = 180$ .

The simplified phase term was found to be

$$r - \bar{\rho} \cdot \bar{R}_1 - S \simeq - P - \varepsilon_t \sin\theta \cos(\phi - \phi_0) - \varepsilon_z \cos\theta \tag{40}$$

where

$$P = r \sin\Psi \left( \sin\theta\cos\Phi \cos\phi \cos\theta_0 + \cos\theta \cos\Phi \sin\theta_0 + \sin\theta \sin\phi \sin\Phi \right) \tag{41}$$

For the current distribution method, equation (29) will reduce to

$$I_L = \int_0^{\theta_c} \int_0^{2\pi} (\bar{n} \times \bar{H}_i) \cdot \bar{L} \exp[-jk(P+S)] \frac{r^2 \sin\theta}{\cos\frac{\theta'}{2}} \, d\theta \, d\phi \tag{42}$$

with equation (31) for the co-polar and the cross-polar radiation fields remaining the same with equation (42) describing $(I_x, I_y)$ .

For the aperture field methodequation (35) defining the Fourier transform integral , reduces to

$$F_i(\Psi, \Phi) = \int_0^{\theta_c} \int_0^{2\pi} \varepsilon_i \exp[\, -jk\,(P+S)\,] \quad r^2 \sin\theta \; d\theta \; d\phi \qquad (43)$$

Similar to the first method equation (34) describing the co-polar and the cross-polar radiation fields, remains unchanged except that equation (43) describes $F_p(\Psi,\Phi)$ in this case.

As the above expressions show, this method is an approximate one. However, it can predict the far field radiation from offset reflectors antennas quite accurately. It can also accommodate small offsets in the primary feed location and thus can be usefully employed in the study or design of multiple beam antennas. This method also succeeds in predicting the beam peak angle position quite accurately even for large displacements.

## 4.3 THE VECTOR CURRENT METHOD

In the previous section, the radiation pattern of offset paraboloid antennas with offset feeds was calculated by the scalar method, which was shown to be an approximate method suitable only for small displacements in the feed with respect to the focal length.

In this section, the radiation pattern is calculated by a new approach which is the vector current method. This method has been applied before only to the case of the axi-symmetric paraboloid with offset feeds and will be extended in this section so it may be applied to offset paraboloid reflectors .

This method is more accurate than the scalar method for it no longer assumes that the magnitude of the primary feed after displacement is equal to its value when the feed was located at the focus. The primary feed radiation is calculated according to its new location. This is achieved by assuming a new rectangular coordinate system $x_3, y_3, z_3$ its origin being the new location of the feed and its $z_3$ axis passing through the vertex of the reflector as shown in figure (6.c). This is assumed, so that the feed is always pointed at the vertex to minimize the spillover.

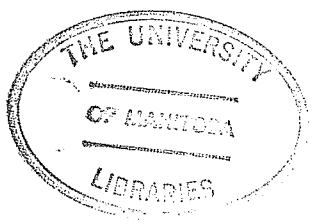

To generalize the calculations and make use of equations derived before, the primary feed radiation $H_i$ is calculated with respect to the $x',y',z'$ axis which is the same coordinate system used in equation (31). To achieve this, the transformation from one co-ordinate system to another has to be known for any possible feed displacement.

To calculate the relation between the $x',y',z'$ and the $x_3, y_3, z_3$ coordinate systems, one shift and two rotations are necessary. First, the $x',y',z'$ axes are shifted by $\varepsilon_x$ , $\varepsilon_y, \varepsilon_z$ respectively, where ( $\varepsilon_x$, $\varepsilon_y$, $\varepsilon_z$ ) are the coordinates of the feed after displacement, figure (6.a). Then, the $z_1 y_1$ plane is rotated by an angle $\eta$ , the amount of which is determined such that the vertex of the reflector will always lie in the $z_1 x_1$ plane, figure (6.b). Finally the $z_2 x_2$ plane is rotated by an angle $\Psi_0$ such that the $z_3$ axis will pass through the vertex, figure (6.c). Equations governing the relation between the two coordinate systems and giving the values of $\eta$ and $\Psi_0$ are derived in Appendix (C).

The radiation pattern of the offset reflector with offset feed is calculated from equation (31) , where $I_x$ and $I_y$ in this case are given by

$$I_L = \int_0^{\theta_c}\int_0^{2\pi} (\bar{n} \times \bar{H}_i) \cdot \bar{L} \quad \exp[-jk(r_3 - \bar{\rho}_3 \cdot \bar{R}_1)] \quad \frac{r^2 \sin\theta}{\cos\theta'/2} \quad d\theta \; d\phi \qquad (44)$$

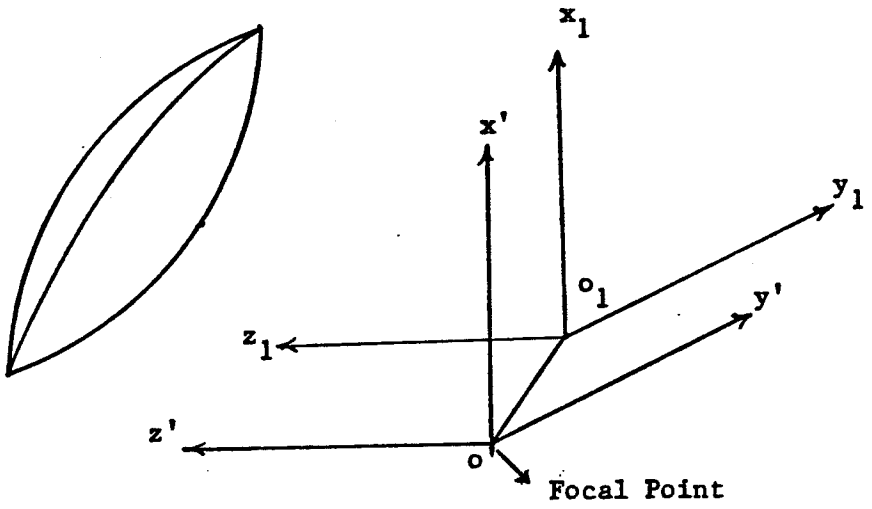


a. The shift of the axes from 0' to $0_1$

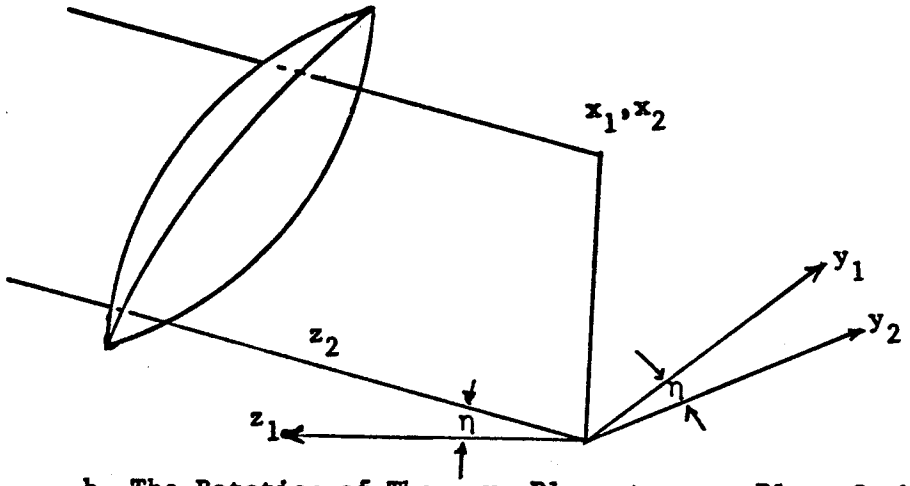


b. The Rotation of The $z_1y_1$ Plane to $z_2y_2$ Plane Such That The $z_2x_2$ Plane Becomes The Reflector Plane of Symmetry

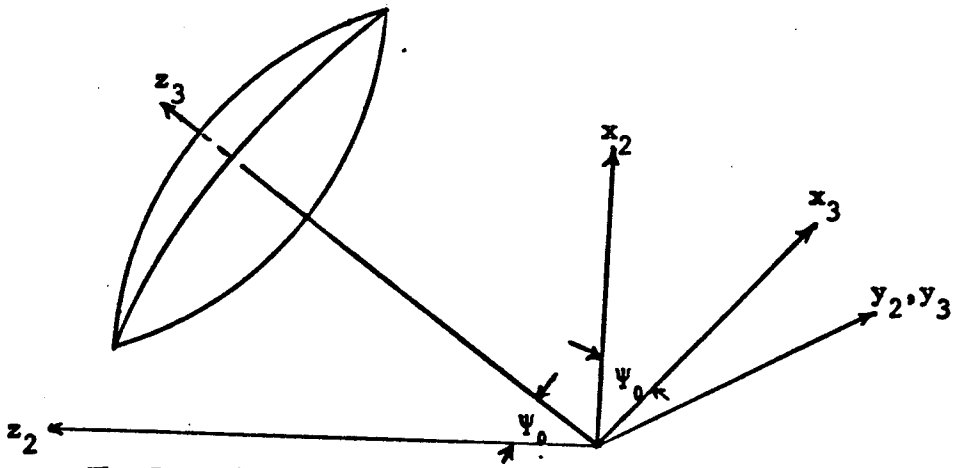


c. The Rotation of The $z_2x_2$ Plane, So That, $z_3$ Becomes The Reflector Axis of Symmetry.

Figure 6. The Shift and The Rotation of The Axes.

where L is x′ or y′

$H_i$ is the primary feed radiation calculated with respect to the x′,y′,z′ as discussed previously.

$\rho_3$ is the vector from the feed location after displacement to a point on the reflector surface as shown in fig (6.c). Its value is given in Appendix (C).

The value of the exponential can be simplified as follows.

where

$$\bar{\rho} = \bar{\varepsilon} + \bar{\rho}_3$$

then

$$\bar{\rho}_3 \cdot \bar{R}_1 = \bar{\rho} \cdot \bar{R}_1 + \bar{\varepsilon} \cdot \bar{R}_1 \quad .$$

As the value of $\bar{\varepsilon} \cdot \bar{R}_1$ is not a function of $\theta$ or $\phi$ , it does not affect the value of the integration and the phase term could be reduced to $r_3 - \bar{\rho} \cdot \bar{R}_1$ . A possible approximation to save some computer storage, is to take the value of $r_3$ similar to that calculated in Appendix (B), namely

$$r_3 \cong r \left[ 1 - \varepsilon_t \sin\theta \cos(\phi - \phi_0) - \varepsilon_z \cos\theta \right] \qquad (46)$$

The phase term will be similar to that of the scalar aperture method represented by equation (40).

# Chapter V

# COMPUTED RESULTS FOR REFLECTOR PATTERNS

## 5.1 INTRODUCTION

In this chapter the computed radiation patterns of an offset reflector with an offset feed are presented. To reduce the computation time a small reflector with an aperture diameter of $d=23.1\lambda$ is selected. The feed is a dual mode circular waveguide, which uses the combination of a dominant $TE_{11}$ and the compensating $TE_{21}$ modes as discribed in chapter I. The reflector has an offset angle of $30^0$ and $f/d=0.866$. The performance of this reflector, for a circular waveguide feed with a mode mixing ratio of $TE_{11}/TE_{21}=0.07$, is investigated by both the current distribution and the scalar aperture methods. The computed patterns by the vector current method are presented, and a comparison between the results of the two methods is discussed.

## 5.2 NUMERICAL INTEGRATION

There is a wide variety of numerical routines which can be used to evaluate two dimensional integrals of the type given in (43) and (44). However, the choice of an optimum routine will be dependent upon the particular type of integral and the range of its application. The critical factor

of accuracy versus the computational time and storage requirement will favour different techniques under different conditions and weights. No single technique appears to be superior in all cases [21].

The commonly used integration techniques may be classified into two groups. The formulas that employ the functional values at equally spaced base points, and the formulas that employ unequally spaced base points, determined by certain properties of the orthogonal polynomials. The first group of numerical integration methods, or quadrature methods include integration algorithms like trapozoidal, Simpson, and Romberg. The second groups are generally referred to as the Gaussian type and use many different types of algorithms depending upon the orthogonal polynomial used [24].

The first group of methods, using values of the functions at equally spaced points, assign constant weighting factors to every value. Conversely, the second group of methods involve functional weighting factor to the function values evaluated at unequally spaced points. The weights for these methods are determined to achieve a maximum order of accuracy. Many different types of polynomials are used to obtain the abscissas for Guassian quadrature formulas, depending upon the type of integrand and the limit of integration.

Lessow et al [25] described a comparison between a number of numerical integration techniques. Their conclusion was that for the main lobe and near sidelobes the most efficient method seems to be the Romberg integration, carried out consecutively on the inner and the outer integral. For further out lobes the Simpson method seemed to be preferable as well as in the cases where extremely high accuracies are required. This problem was later extended by Chugh et al [24] to include Gaussian integration as well. It was shown that for a fixed number of integration points, normally the Gaussian algorithms are more accurate. However, in using these methods to carry out integrations with a prescribed degree of accuracy the Simpson method becomes compatible with the Gaussian quadrature method. This is due to the fact that in Simpson's rule to increase the accuracy of the integration one only needs to add the contribution of the new points to that of the previous ones. Gaussian quadratures, however, need a complete reevaluation of the integral, which increases the computation time.

In many cases to save a considerable amount of computational time, specially for large off-axis angles, different approximate techniques such as the stationary phase method are used. These methods are usually applied to eliminate the azimuthal $\phi$ integration and only the $\theta$ integration would remain, which is performed numerically. However, the

results of the stationary phase method are only applicable for cases where the feed is located at the focus of the reflector. Here we are interested in evaluating the diffraction patterns of the offset reflectors for offset feeds, where the feed is no longer at the focus. Furthermore, we may also wish to study the performance of the offset reflectors for arbitrary feeds. In such cases, the stationary phase approximation is too complex to utilize and requires the evaluation of the integral for each new feed. Thus for such cases, performing the double integration becomes more favourable.

In this thesis the double integrations in equation (43) and (44) are performed by applying Simpson's rule. To overcome the problem of excessive computation time, required by two dimensional integration, we have utilized additional computer storage to eliminate many repeated evaluations of the feed patterns and other special functions present in the diffraction integral. To clarify, we note that for evaluation of the reflector patterns, for several different cases, the feed pattern and the exponential function are computed repeatedly for the same $\theta$ and $\phi$ variables. Therefore, to reduce the computational time, these functions are computed for all required values $\theta$ and $\phi$ and are stored for latter use. The reflector pattern calculations then reduces to summation of the already computed data. In this manner the

computation of the two dimensional integrals can be carried out quite efficiently . In fact, this computer program requires computation time comparable with that based on the stationary phase approximation for offset reflector with feed at the focus, which requires a single numerical integration [9].

## 5.3 THE BEAM FACTOR

When a beam is scanned off axis in a paraboloid, its angular position is smaller than the angular displacement of the feed horn. The ratio between the two angles is called the beam factor. Lo [26] studied the beam factor for the axisymmetric paraboloid and found that it depends on the edge illumination and on f/d ratio of the reflector. He has shown that for large f/d ratios, the beam factor approaches unity.

Similar to the axisymmetric paraboloid, the beam factor in the case of an offset paraboloid, may be defined as the ratio of the beam deflection angle $\Theta_b$ to the angular displacement of the feed $\Theta_f$ , both measured from the axis of the reflector with its vertex as the origin, as seen in figure (7). From figure (7) it can be seen that;

$$\Theta_f = \tan^{-1}\left(\frac{\varepsilon_n}{f'}\right)$$

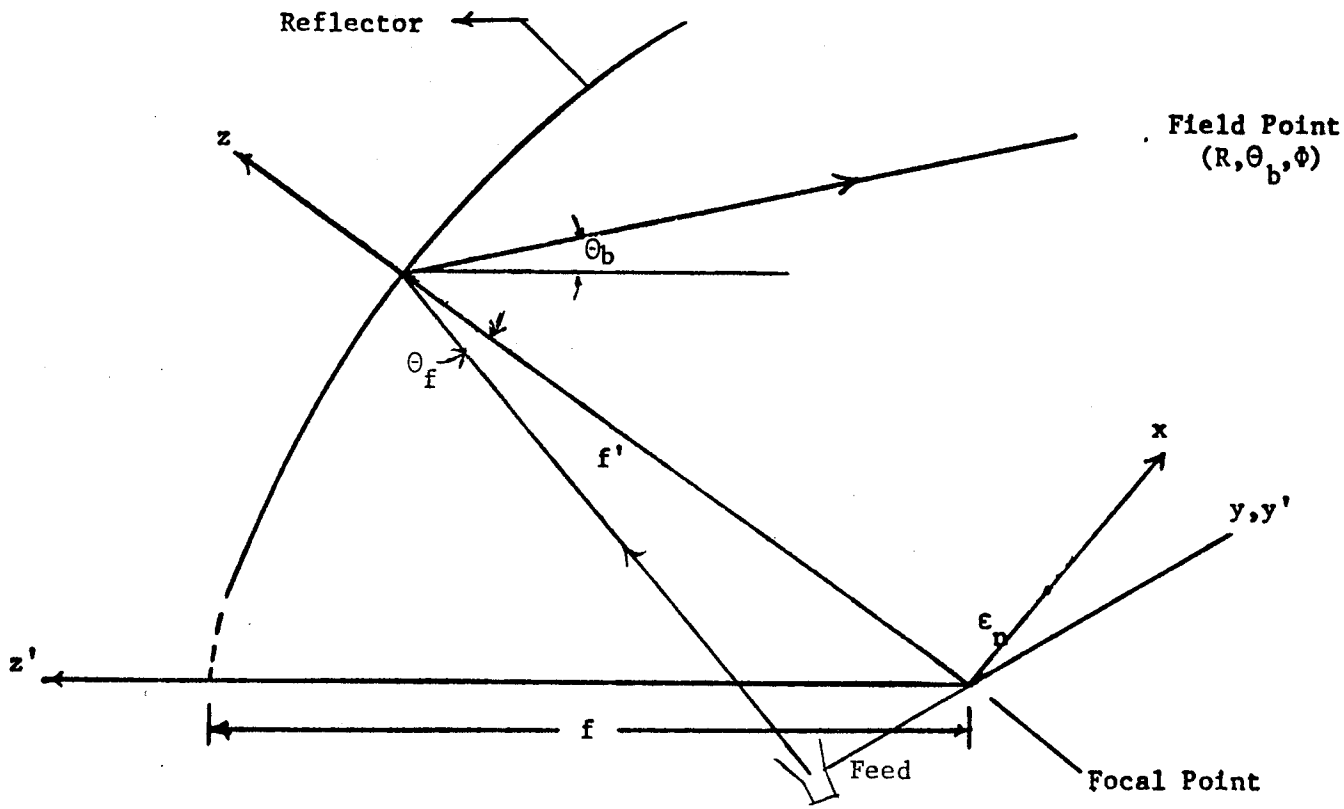


Figure 7. The Geometry for The definition of the Beam Factor

where $\epsilon_n$ is the shift of the feed along either the x or the y direction, and

$$f' = \frac{2f}{1 + \cos\theta_0}$$

This definition was used in this thesis to calculate the beam factor of the offset reflector under investigation. As an example, for a $2\lambda$ displacement of the feed along the x-axis, the beam shift was found to be $5^0$ for which the beam factor becomes ;

$$B.F = \frac{\theta_b}{\theta_f} = \frac{5^0}{\tan^{-1}\frac{2\lambda}{f'}} = \frac{5}{5.33} = 0.938$$

## 5.4 COMPUTED RESULTS AND DISCUSSION

This section presents the computed patterns for various offsets feed locations. The computed patterns are for a reflector with an aperture diameter of $d=23.1\lambda$ , $f/d=0.866$ , and an offset angle of 30 degrees.

The patterns are computed from equation (31) for the case of vector current method, using Simpson's rule. The feed offsets along the x and the y axes are considered and the computed patterns are presented for the co-polar and the cross-polar radiations in the planes of symmetry and asymmetry of the reflector.

### 5.4.1 Shift Along The X-Axis

Figure (8) shows the gain of the reflector in the plane of symmetry, $\Phi = 0$ and for feed offsets along the x-axis. The computed gains of both scalar and vector methods are produced in this figure. However, since the results of the vector current method are more accurate, they will be discussed first in the following sections. A comparison between the results of these methods will be made in a later section. It is seen from the figure that shifting the feed along the postive x-axis slightly increases the gain of the reflector, and the maximum gain is reached at $\epsilon_x = 1.5\lambda$. As the feed is shifted further along the postive x-axis, the gain starts to decrease. On the other hand, shifting the feed along the negative x-axis results in a rapid decrease of the gain. The results of figure (8) indicates that the gain drops from 35.89 dB, in the case of no shift, to 35.56 dB, that of a $2\lambda$ feed offset along the negative x-axis. The change of the gain with the displacement along the x-axis is due to the defocussing effect. However, shifting the feed along the positive x-axis increases the distance of the feed from the reflector, and the defocusing effect becomes less severe than the case of shifting the feed along the negative x-axis.

Figure (9) shows the diffraction patterns of the reflector for feed shifts along the x-axis and equal to $0, \lambda, 2\lambda$.

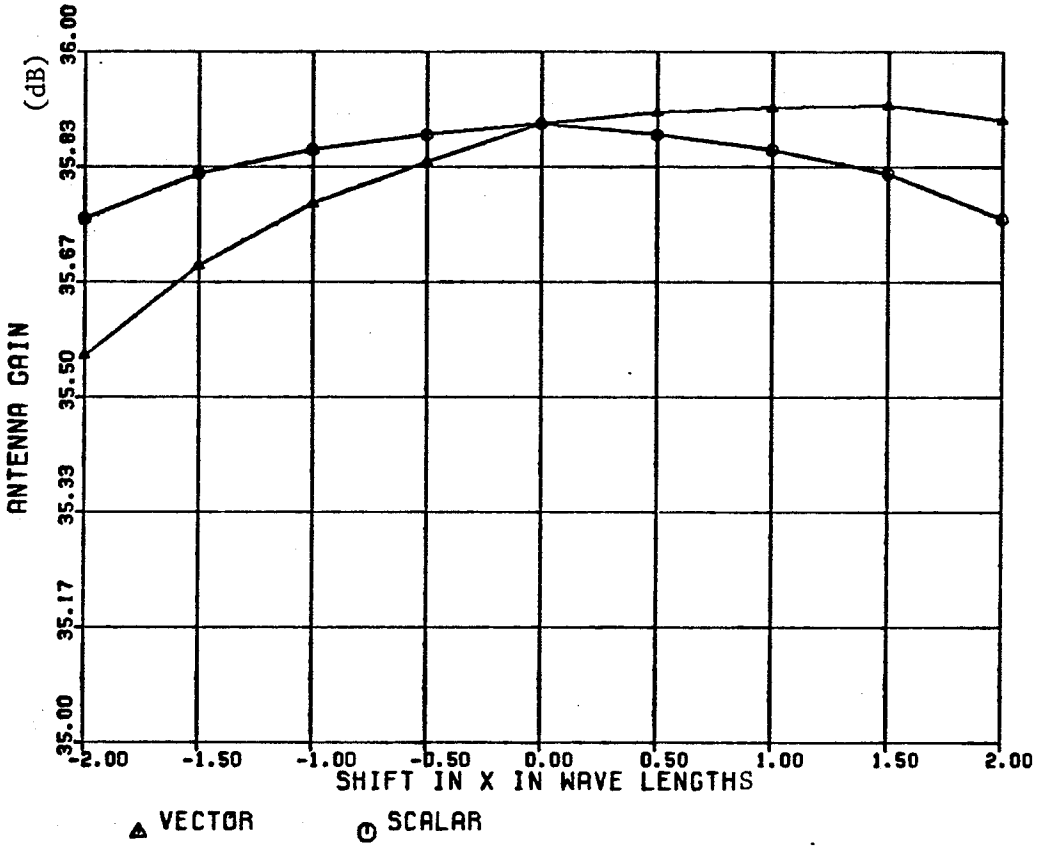


Figure 8. The Computed Gains of The Reflector by both The Vector Current Method and The Scalar Aperture Method as a Function of The Feed Displacement Along The x-axis.

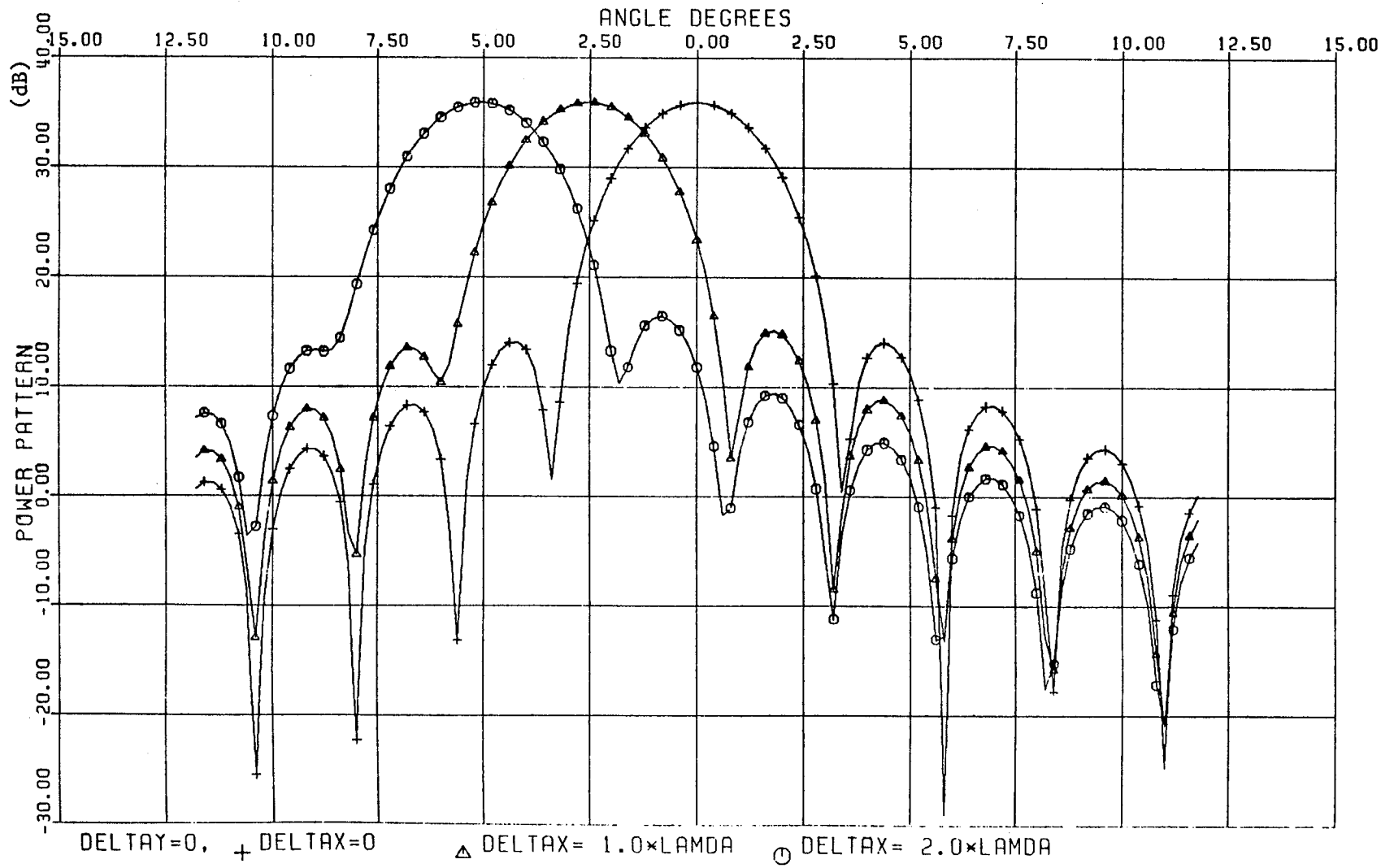


Figure 9. The Co-polar Patterns of The Reflector for Feed Displacements Along The x-Axis, Plane of Symmetry.

Shifting the feed along the x-axis shifts the direction of the main beam away from the reflector's z-axis. The amount of this shift is proportional to the feed displacement and the reflector indicated a beam factor of about 0.938. This indicates that the amount of the beam shift is about 0.938 times the angular shift of the feed as seen from the reflector centre. For the assumed reflector a shift of $5^0$ in the beam can therefore be achieved by a feed displacement of about $2\lambda$ .

While shifting the feed along the positive x-axis shifts the beam in the $\Phi = \pi$ plane, the shift along the negative x-axis shifts the beam along the $\Phi=0$ plane. It could also be seen from figure (9) that the shift of the beam also increases the side lobe levels. However, this increase is not symmetric with respect to the beam axis. On the feed side (right hand side in figure 9) the side lobes increase with the shift, whereas, away from the feed they tend to decrease, as the feed offset increases.

The cross polarization level in the plane of symmetry and for shifts along the x-axis was found to be negligible, and its patterns are not included. This is due to the fact that the feed is symmetrically located with respect to the reflector and does not contribute to cross-polar radiations for patterns in the plane of symmetry.

It was found that shifting the feed along the x-axis does not affect significantly the co-polar patterns in the plane of asymmetry and the computed patterns are not included. Figure (10) shows the cross polarization level in the plane of asymmetry due to shifts along the x-axis computed by both the vector current and the scalar aperture methods. Considering the results of the vector current method only, it is evident that the level of the cross-polar radiation decreases as the feed displacement increases along the positive x-axis. This decrease continues until a certain value of $\varepsilon_x = 1.5\,\lambda$, beyond which the cross polarization level increases with the increase in the displacement. This may be due to the fact that the feed displacement along the x-axis increases the distance of the feed from the reflector, and the effect of defocusing is less severe. The decrease in the cross polarization level reaches its optimum value for a shift of $1.5\lambda$ along the positive x-axis, beyond which the defocusing is severe and the gain starts to decrease for any additional increase in the feed shift. This relationship is supported by the increase in the level of the cross-polar radiation when the feed is shifted along the negative x-axis, where the shift continuously decreases the feed distance from the reflector. The cross polarization patterns in the plane of asymmetry are shown in figure (11). It could be noticed that for feed shifts along the x-axis, the cross-polar patterns do not shift from the reflector axis with the feed.

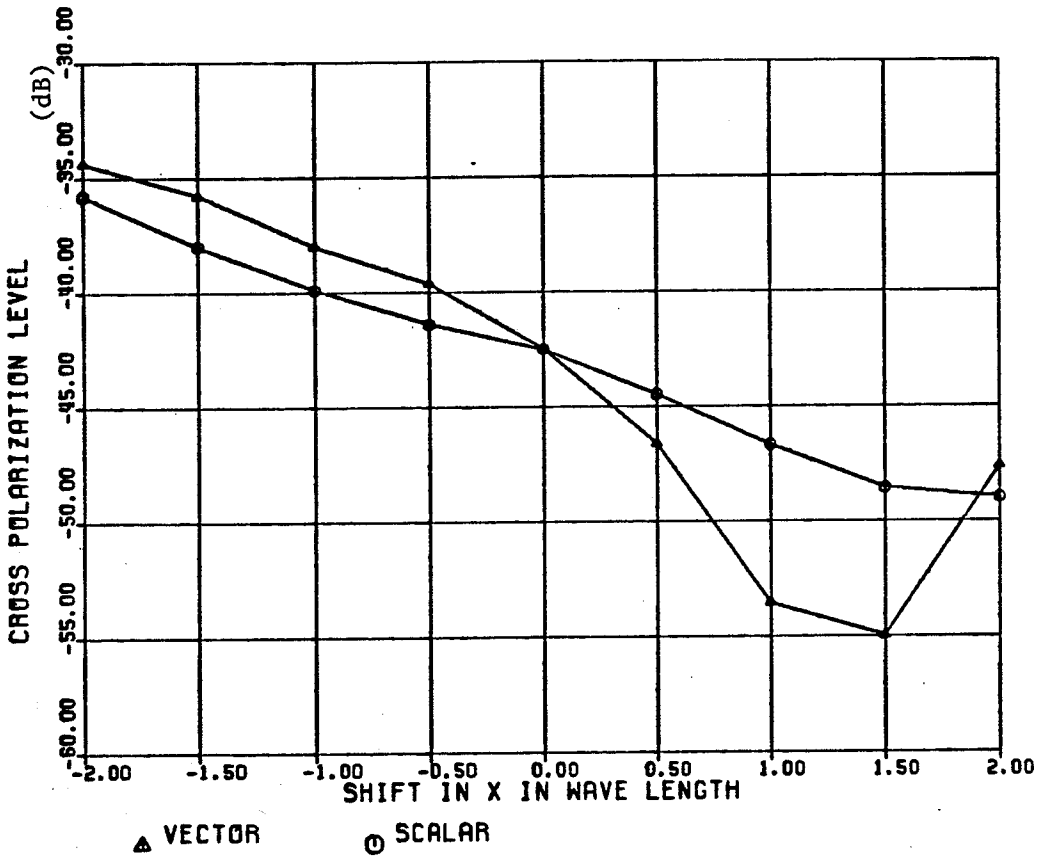


Figure 10. The Computed Cross Polarization of The Reflector by both The Vector Current and The Scalar Aperture Methods, Plane of Asymmetry.

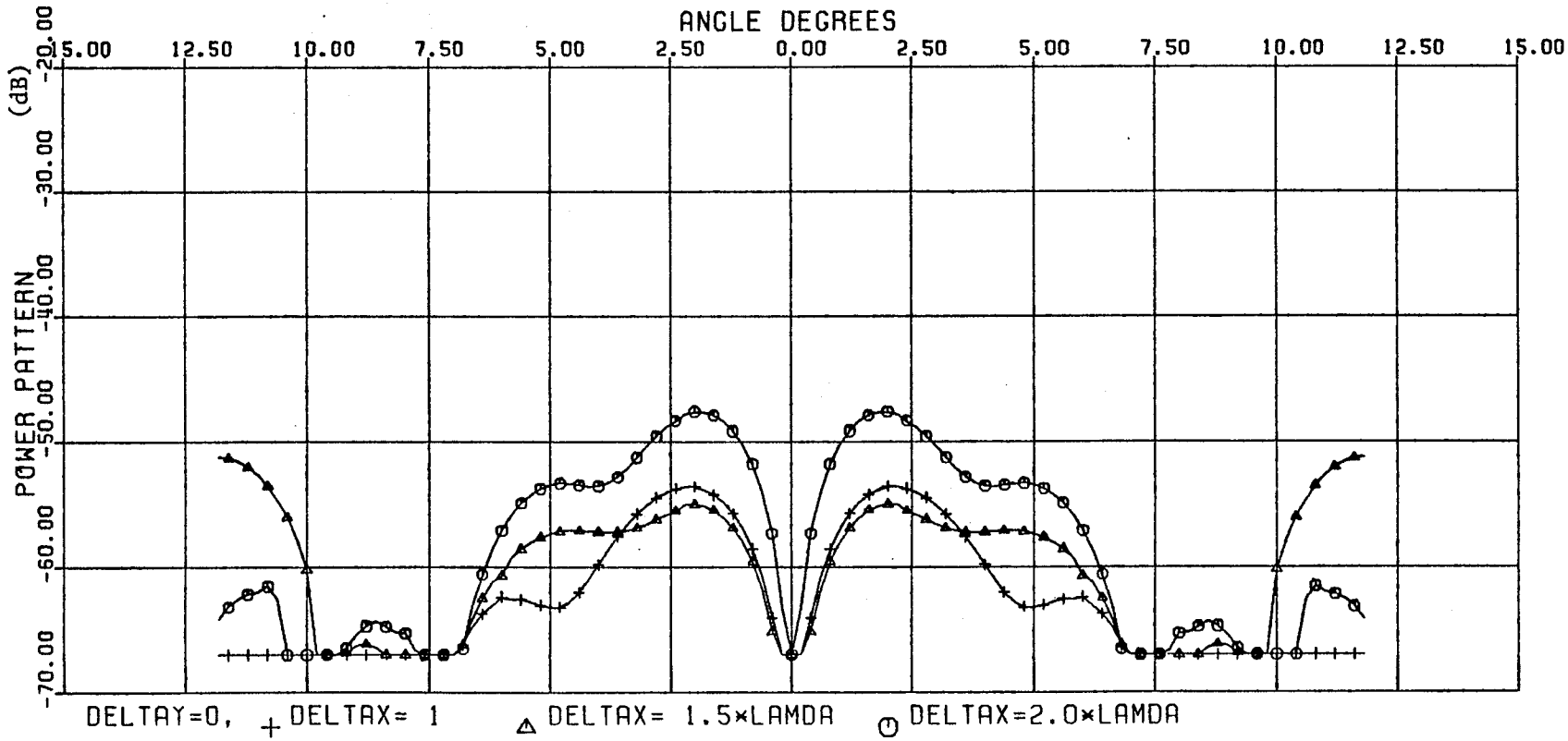


Figure 11. The Cross-Polar Patterns of The Reflector for Feed Displacements Along The x-axis, Plane of Asymmetry.

### 5.4.2 Shift Along The Y-Axis

The co-polar patterns of the reflector in the plane of asymmetry and for feed dislocations along the y-axis are shown in figure (12). Comparing the results with those of figure (9), representing the radiation patterns in the plane of symmetry with shifts along the x-axis, we note that the amount of the beam shifts are equivalent, which indicates the similarity of the feed displacements along both the x and the y axes. The main difference between these two shifts is in the level of coma lobes. For displacement along the x-axis, it seems that the asymmetry of the geometry corrects the illumination and the coma lobes are less significant. The side lobes of the reflector are therefore almost symmetrical about the main lobes. On the other hand, since the geometry of the reflector is symmetric about the x-axis, a displacement of the feed along the y-axis destroys the symmetry of the feed and the coma lobes becomes significant. It could also be seen from figure (12) that there is a small decrease in the gain of the reflector as the shift increases, however, this decrease is not significant.

For the feed displacement along the y-axis, the feed is no longer symmetric with respect to the reflector and cross polarization exists. The computed results in the asymmetrical $\Phi = \frac{\pi}{2}$ Plane are shown in fig (13). These results indicates that the cross polarization patterns also shift from

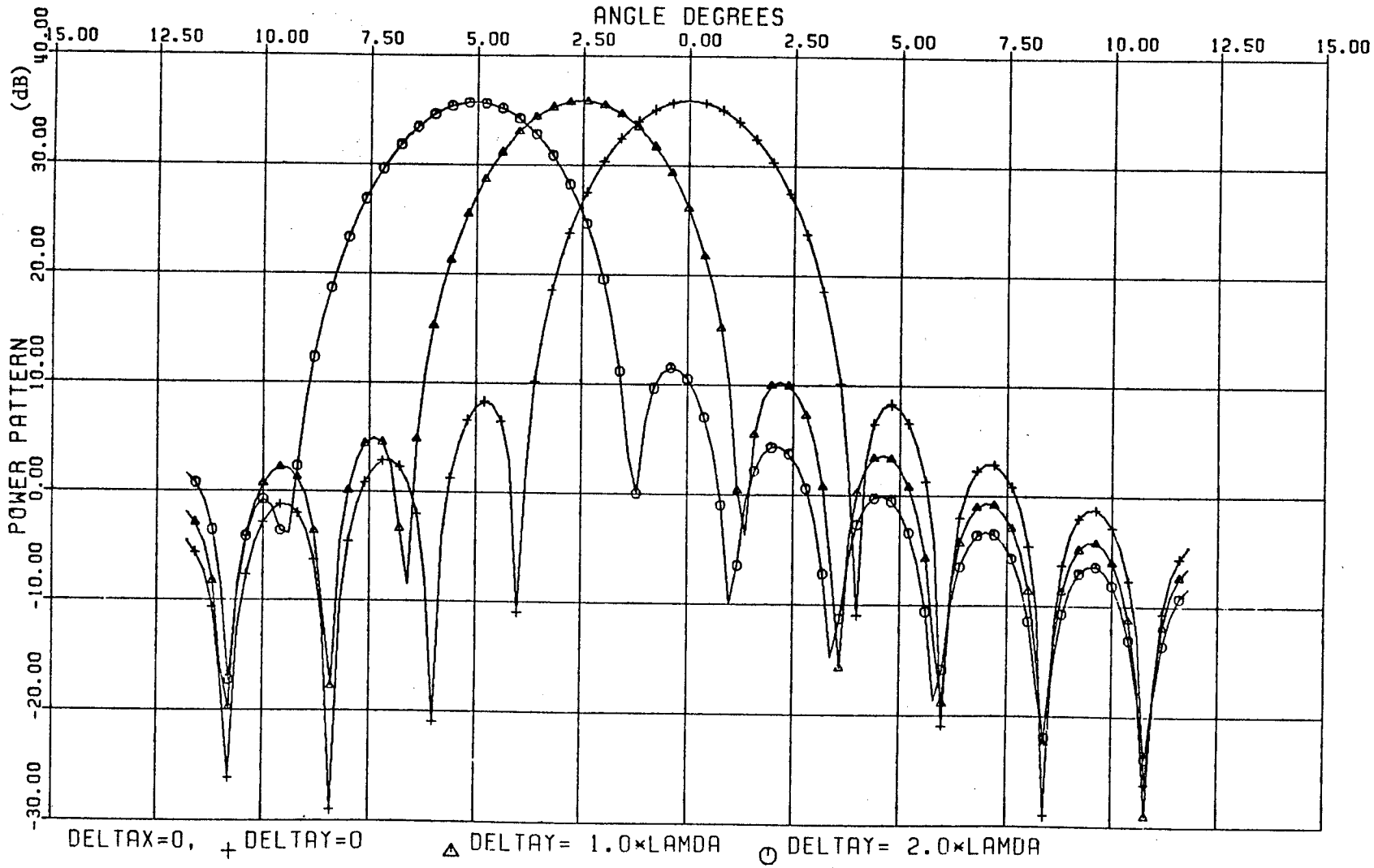


Figure 12. The Co-Polar Patterns of The Reflector for Feed Displacements Along The y-axis, Plane of Asymmetry.

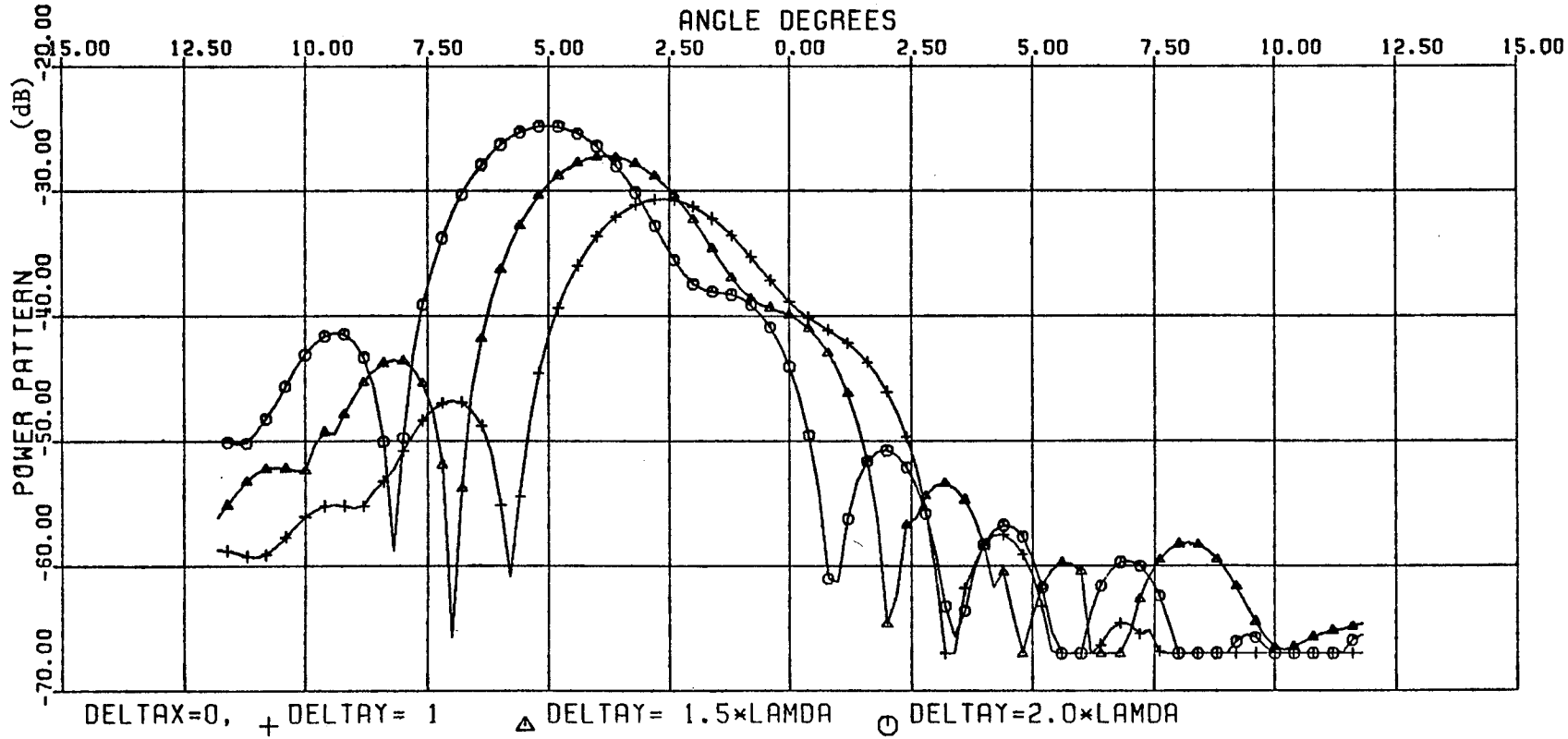


Figure 13. The Cross-Polar Patterns of The Reflector for Feed Displacements Along The y-axis, Plane of Asymmetry.

the reflector axis, by the same amount as the beam shift of the co-polar pattern. This is a disadvantage, especially when a frequency re-use system is required, since the maximum cross polarization occurs in the coverage zone of the main lobe.

Figure (14) shows the cross polarization levels for shifts along the y-axis. It indicates that the level of cross polarization increases continuously as the displacement increases. This increase of the cross-polar radiation may be due to the fact that for the feed displacement along the y-axis the symmetry of the geometry is deteriorated.

Figure (15) shows the reflector patterns in the plane through the beam and the x-axes. It is seen that there is no change in the behaviour of the the co-polar patterns. The only change is the shift of the beam with respect to the z-axis. However, this shift is not observed on the figure, since the pattern is computed with respect to the plane passing through the beam axis. Figure (16) shows the cross polarization level in the plane of symmetry for displacements along the y-axis. The cross polarization increases rapidly as the shift increases, and the angles of the maximum cross polarization are shifted towards the co-polar beam peak. This is a disadvantage, since the maximum

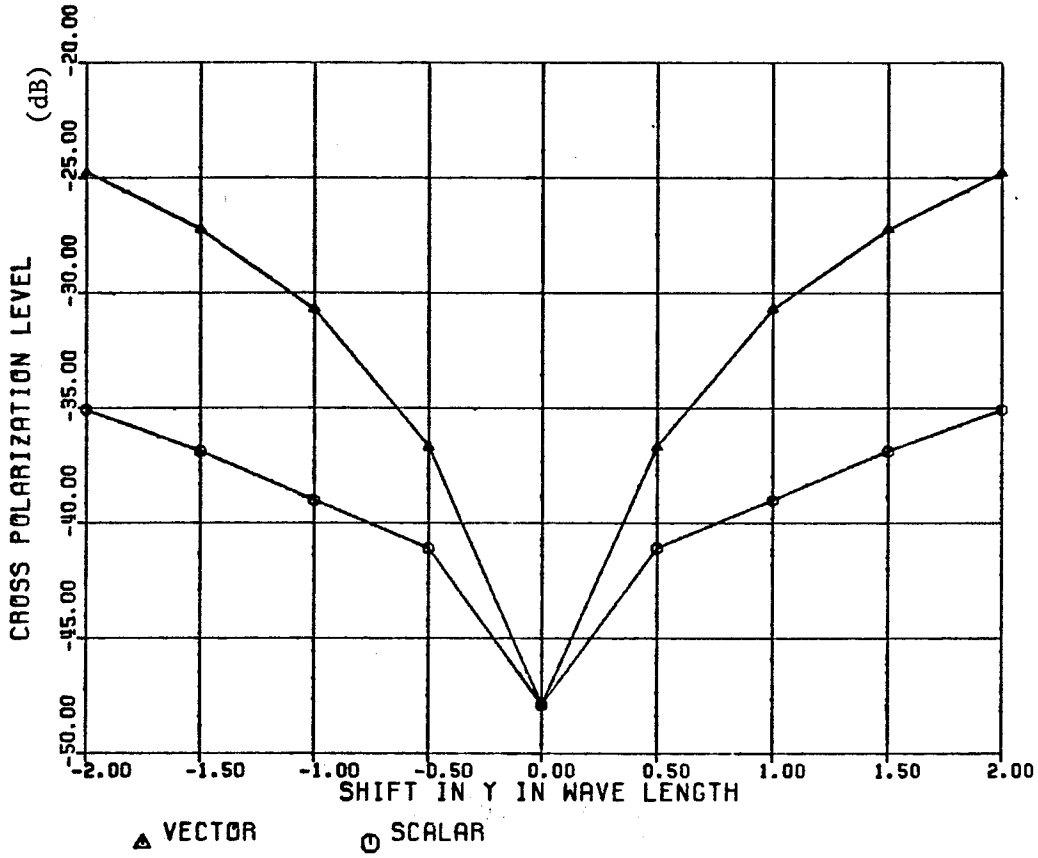


Figure 14. The Computed Cross Polarization of The Reflector by both The Vector Current and The Scalar Aperture Methods, Plane of Symmetry.

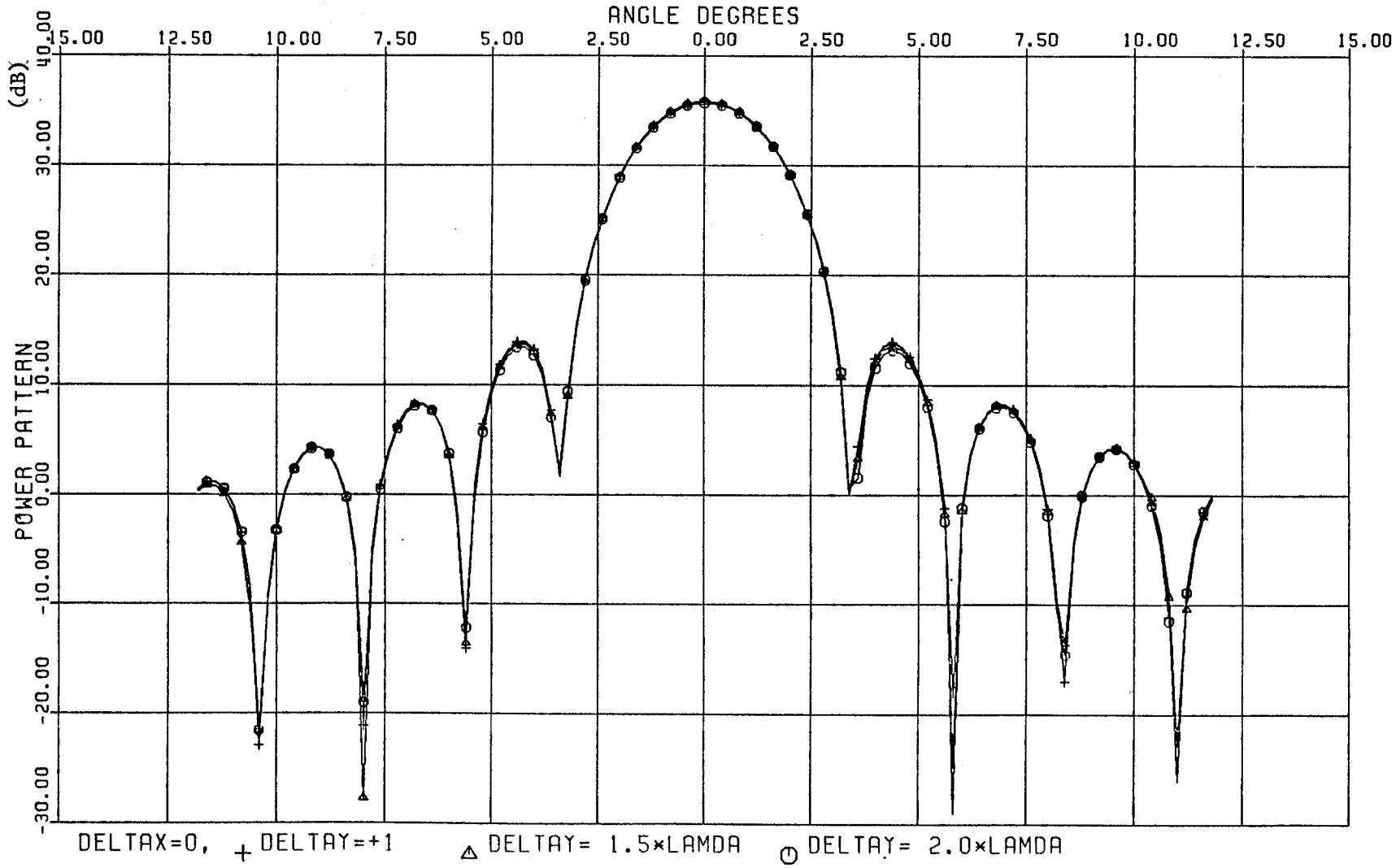


Figure 15. The Co-Polar Patterns of The Reflector for Feed Displacements Along The y-axis, Plane Normal to $\phi=\pi/2$ Plane.

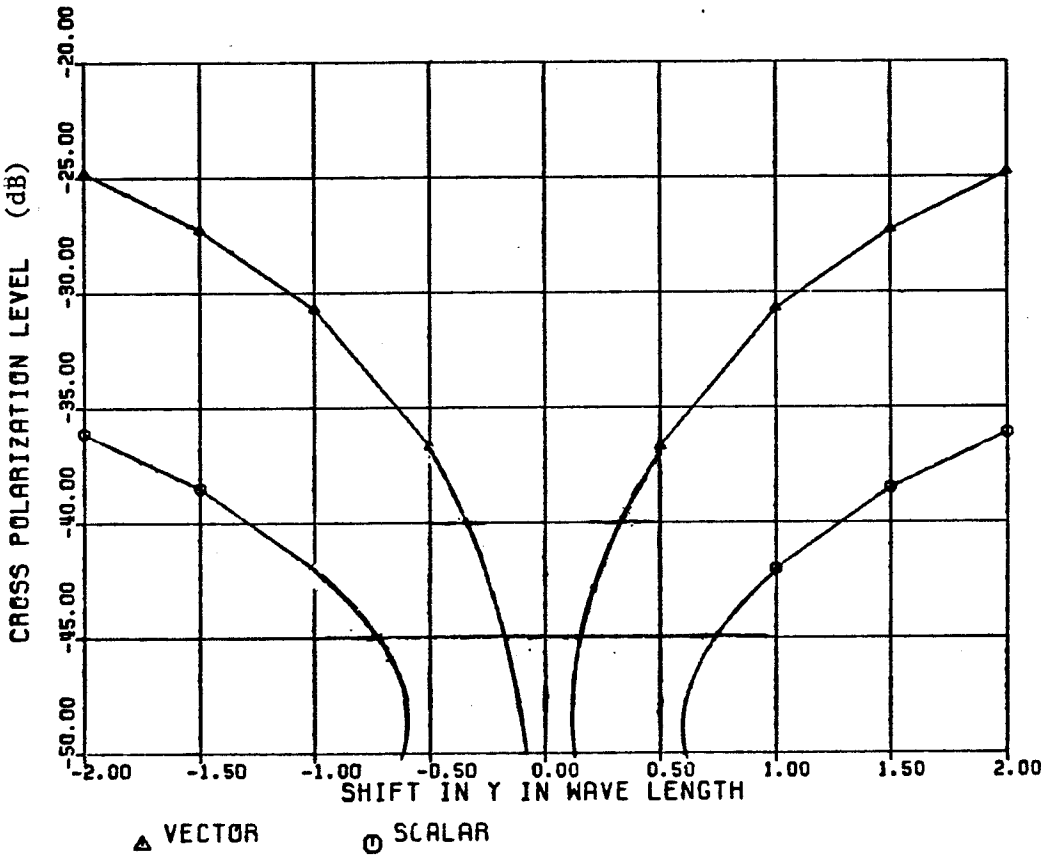


Figure 16. The Computed Cross Polarization of The Reflector by both The Vector Current and The Scalar Aperture Methods, Plane Normal to $\phi=\pi/2$ Plane.

cross polarization occurs in the coverage zone of the main lobe.

Hence, we conclude that the feed displacement along the x-axis not only has a negligible effect on the co-polar pattern, but it also improves the cross-polar radiation of the reflector. Comparing the cross-polar levels due to shifts along both the x and the y axis, it is clear that the highest level of -33 dB for the case of $-2\lambda$ shift along the x-axis, is much lower than -24 dB which is the level of the cross-polar radiation in the case of a $2\lambda$ shift along the y-axis.

## 5.5 COMPARISON BETWEEN THE VECTOR CURRENT METHOD AND THE SCALAR APERTURE ONE

In the previous section, the computed results of the radiation patterns by the vector current method have been presented. In this section a comparison between these patterns and those calculated by the scalar aperture method are discussed for shifts along both the x and the y axes.

### 5.5.1 Shift Along The X-Axis

The scalar method gives a co-polar pattern almost similar to that computed by the vector current method in both the planes of symmetry and asymmetry, except that the latter gives slightly higher side lobes. However, the difference in the level of the side lobes is not significant. On the

other hand, the vector current method showed an increase in the gain as the shift along the postive x-axis increased, while similar shifts slightly decreased the gain of the reflector in the scalar method as seen in figure (8).

The vector current method gave slightly different patterns for shifts along the negative x-axis than that of the same shift along the positive x-axis. However, the scalar aperture method predicted that they should be similar. This is due to the approximations assumed in the scalar method.

The cross polarization levels in the plane of asymmetry computed by both the vector current and the scalar aperture methods were shown in figure (10). An examination of this figure shows that both methods predict a low cross polarization level. However, the scalar method predicts a steady decrease in the cross polarization level as the shift increases along the positive x-axis. Conversely, the decrease in the cross polarizarion level predicted by the vector current method reaches a minimum when the feed shift reaches about $1.5\lambda$. Any further increase in the feed shift will result in an increase of the cross polarization level.

### 5.5.2 Shift Along the Y-Axis

Figure (17) shows the co-polar pattern in the plane of asymmetry for a shift of $2\lambda$ along the y-axis, computed by both

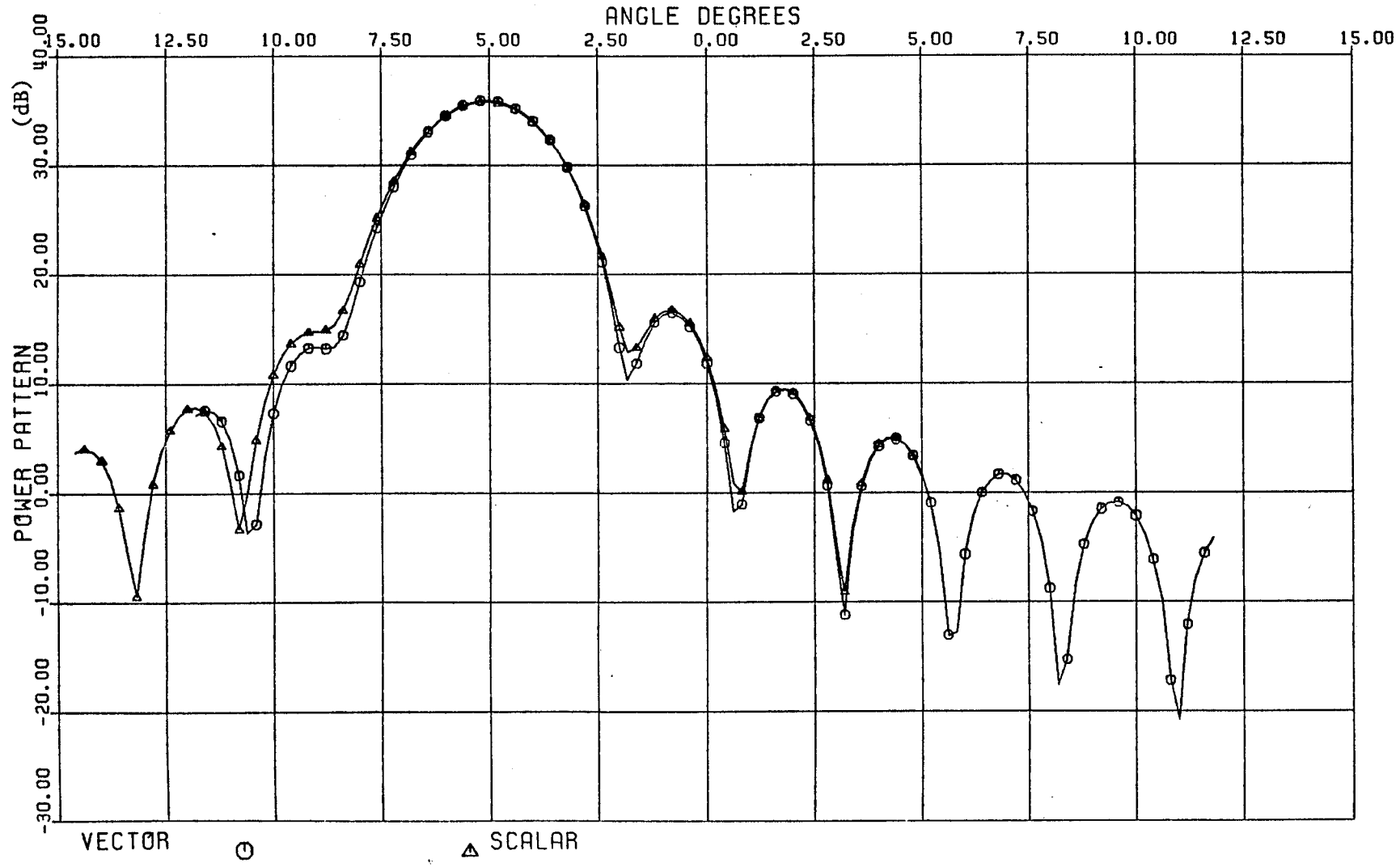


Figure 17. The Co-Polar Patterns of The Reflector by both The Vector Current and The Scalar Aperture Methods and for a Shift of 2λ Along The y-axis, Plane of Asymmetry.

the vector current and the scalar aperture methods. It could be seen that both methods predicted almost similar patterns, with the scalar method predicting higher side lobes in the reflector side of the plane. Similarly both methods predicted almost a similar pattern in the plane of symmetry and the computed patterns are not included. The cross-polar patterns are quite different, as may be seen in figures (18) and (19). They show the cross-polar patterns of both methods in the planes of symmetry and asymmetry respectively and for a shift of 2 $\lambda$ along the positive y-axis. The level of the cross-polar radiation were shown in figures (14) and (16). It is seen from these curves that the vector current method always predicts a higher cross polarization level. Also, figure (19) shows that the vector current method predicts a shift in the cross-polar beam similar to that of the co-polar pattern. Nevertheless, the scalar method predicted a much smaller shift.

## 5.6 APPLICATION OF THE RESULTS FOR LARGE REFLECTORS

As mentioned previously, to reduce the computation time, a small reflector of $d=23.1\lambda$ with $f/d=0.866$ was selected. However, since the utilized physical optics approximation improves for large reflectors, the presented results can be used for any large reflector. It only remains to modify the horizontal axis, for the angle, so that the results can be utilized for other reflectors. In such a case, the required

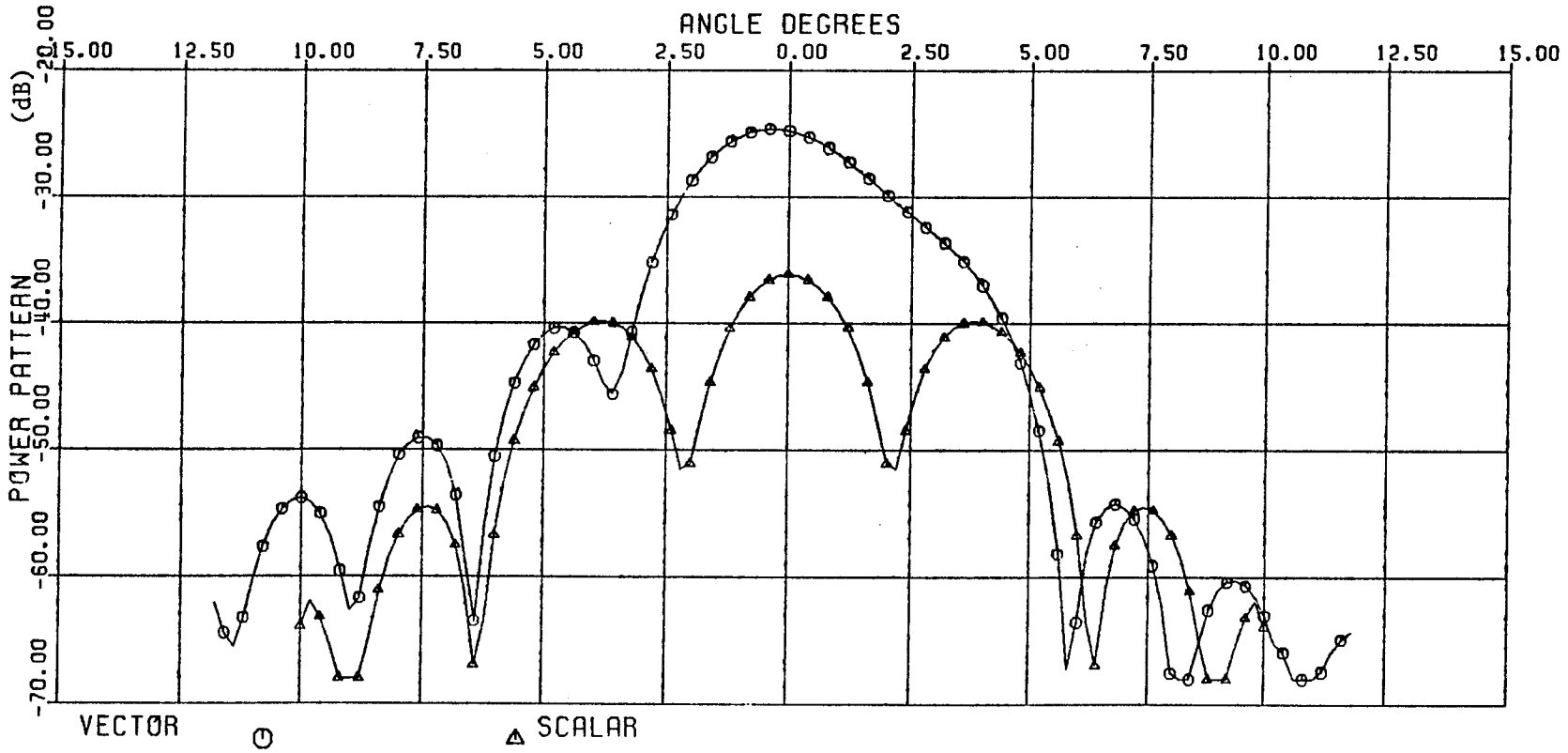


Figure 18. The Cross-Polar Patterns of The Reflector by both The Vector Current and The Scalar Aperture Methods and for a Shift of 2λ Along The y-axis, Plane of Symmetry.

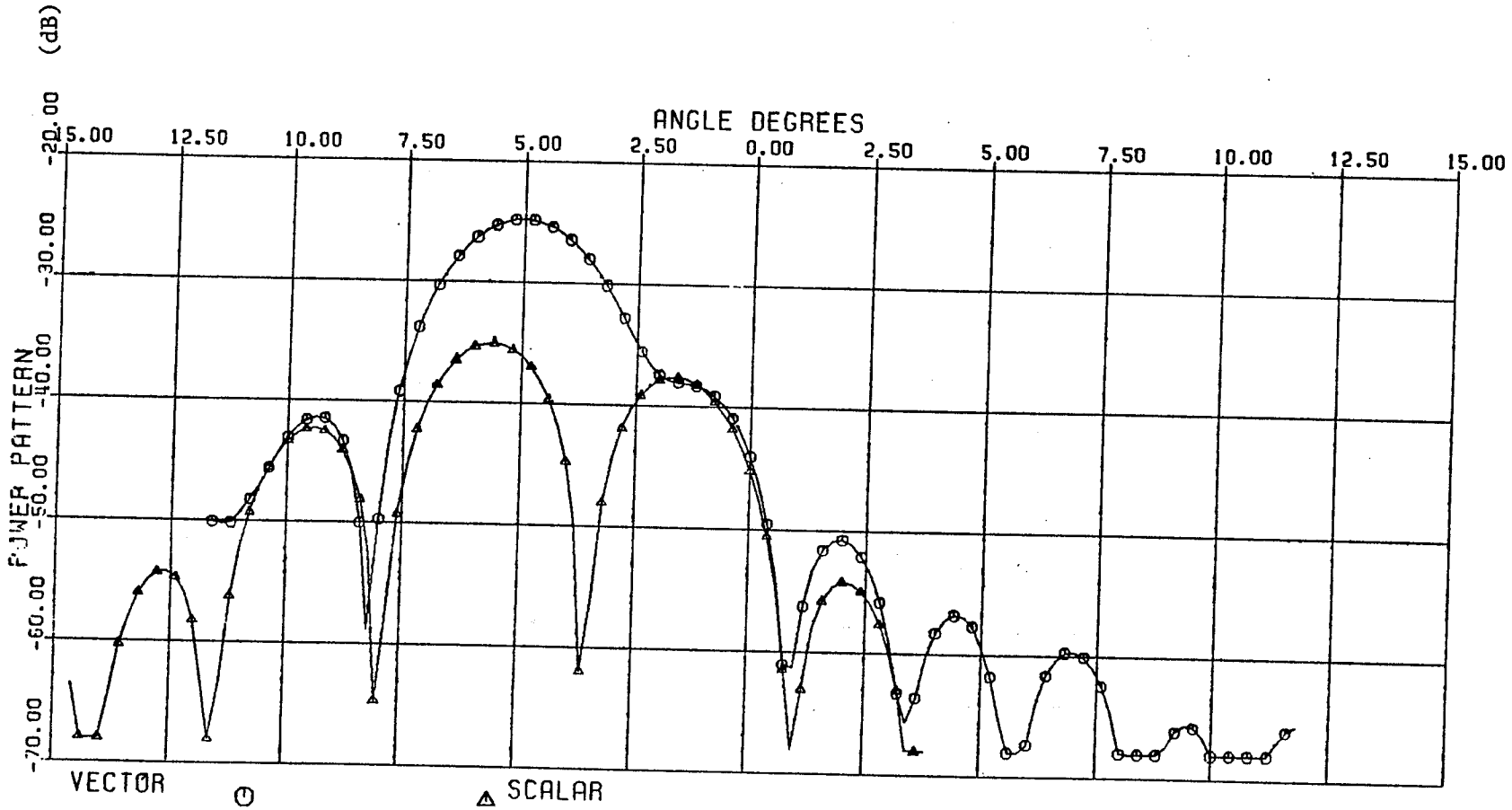


Figure 19. The Cross-Polar Patterns of The Reflector by both The Vector Current and The Scalar Aperture Methods and for a Shift of 2λ Along The y-axis, Plane of Asymmetry.

modification of the horizontal axis may be obtained from $d \sin\theta = d' \sin\theta'$, or $\theta' = \sin^{-1}(d/d' \sin\theta)$, where $d'$ is the aperture diameter of the new reflector and $\theta'$ is the new angle to be used for the horizontal axis of the patterns. As an example, the 3 dB beam width of our $23.1\lambda$ reflector is about 2.8 degrees. If a larger reflector, with a 3 dB beam width of 1 degree is required, its aperture diameter must be $d = 64\lambda$. Our computed patterns can be utilized for this reflector, provided the horizontal axis, for the angle $\theta$, is multiplied by a factor 0.357. The required feed displacements, to yield identical results, must however be multiplied by the factor 2.80. That is, our data, for a feed displacement of $2\lambda$ is equivalent to the results of the new reflector with a feed displacement of $5.6\lambda$ [9].

## 5.7 CONCLUSIONS

This thesis presented the performance of an offset paraboloidal reflector with offset feeds. Mathematical expressions necessary for the computation of the co-polar and the cross-polar radiation fields were obtained and were utilized to compute the far field patterns by both the vector current method and the scalar aperture one. To generalize the problem a computer program was prepared which used a two dimensional integration to compute the required integrals. The computation time, necessary for the pattern calculations was reduced effectively by using additional storage to eliminate

repeated calculations of the feed patterns, the exponential and other special functions. Also, a small reflector, with an aperture diameter of 23.1λ was selected to further economize the computation time. However, the results are still applicable to larger reflectors by using proper scaling factors.

For the reasons mentioned in the introduction, only beam shifts of $\pm 5^0$ were considered. With our reflector this could be achieved by offsetting the feed within $\pm 2^0$ . The computed patterns indicated that generally the co-polar patterns yield antenna gains in the order of the antenna gain, when the feed was located in the focus. The cross-polar patterns, however, gave larger values when the distance of the displaced feed from the reflector was increased. Nevertheless, reduction in the cross-polar radiation level can be achieved by increasing the distance of the displaced feed from the reflector. The computed patterns also indicated that the feed displacement along the x-axis not only has a negligible effect on the co-polar radiation, but also improves the cross-polar radiation of the reflector.

Although the scalar aperture method is an approximate one, it always predicted a co-polar pattern quite similar to that predicted by the vector current method. It also succeeded in predicting the beam peak angle position quite

accurately, even for the largest displacements. However, this method always predicted lower values for the cross-polar radiation than those predicted by the vector current method. The use of this method in the past, has been preferred since it leads to simple mathematical expressions. In this thesis, similar simple expressions have been derived for the vector current method. Thus the computer program which is developed and based on the vector current method requires computation time comparable with that based on the scalar aperture method.

## Appendix A

## TRANSFORMATION OF THE AXIS

The equations governing the transformation from the x,y,z to the x′,y′,z′ coordinate systems, figure (20), are

$$x = x' \cos\theta_0 - z' \sin\theta_0$$

$$z = z' \cos\theta_0 + x' \sin\theta_0$$

$$y = y'$$

$$r' = \sin\theta' \cos\phi' x' + \sin\theta' \sin\phi' y' + \cos\theta' z' \qquad (1)$$

$$r = (\sin\theta \cos\phi \cos\theta_0 + \cos\theta \sin\theta_0) x' + \sin\theta \sin\phi y' + (\cos\theta \cos\theta_0 - \sin\theta \sin\theta_0 \cos\phi) z' \qquad (2)$$

and $\rho \equiv \rho'$

hence by equating equation (1) and (2) it is seen that;

$$\sin\theta' \cos\phi' = \sin\theta \cos\phi \cos\theta_0 + \cos\theta \sin\theta_0$$

$$\sin\theta' \sin\phi' = \sin\theta \sin\phi$$

$$\cos\theta' = \cos\theta \cos\theta_0 - \sin\theta \sin\theta_0 \cos\phi$$

The equation of the paraboloid with respect to the x,y,z axis is;

$$x^2 + y^2 = -4 f(z-f)$$

where f is the focal length of the parent paraboloid.

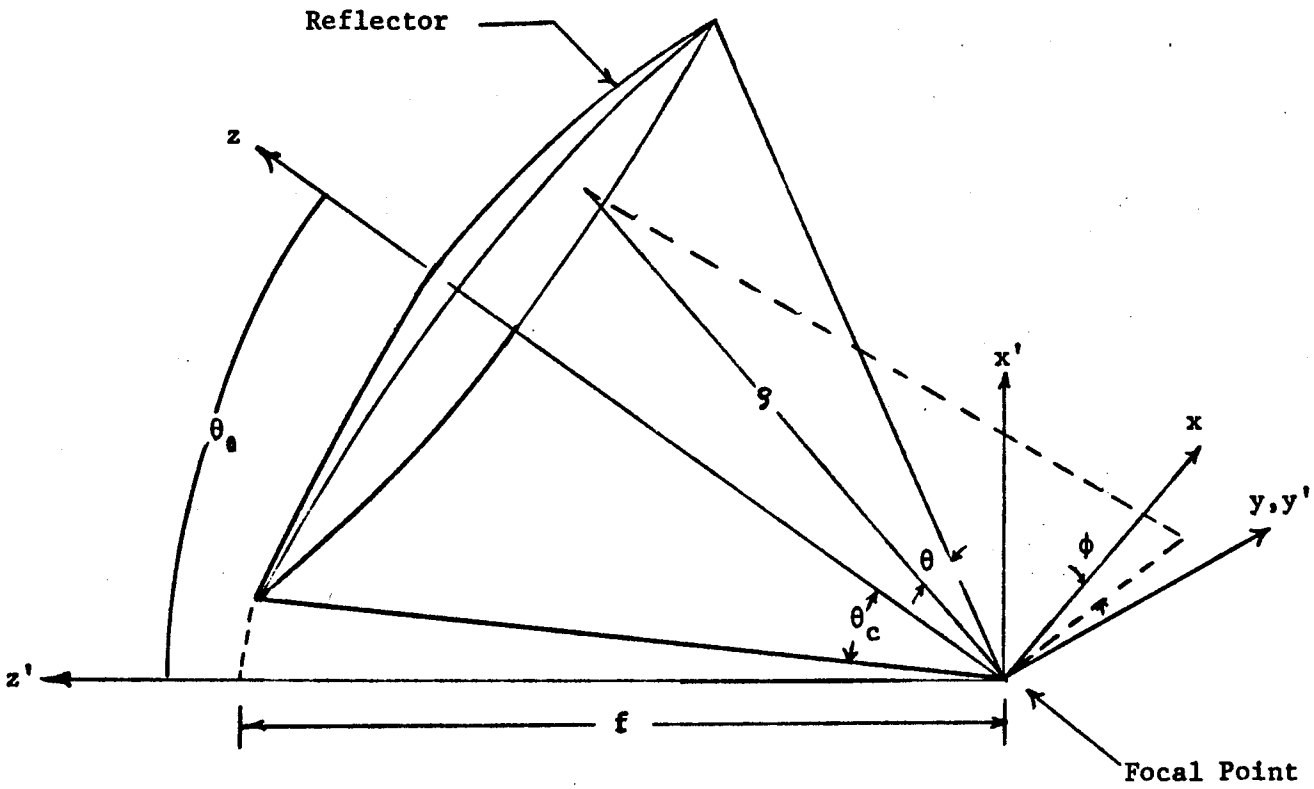


Figure 20. Offset Reflector Coordinate System.

## Appendix B

## PHASE TERM APPROXIMATION

With reference to figure (21)

$$\bar{\rho} = \rho_x \bar{x} + \rho_y \bar{y} + \rho_z \bar{z}$$

$$\bar{\rho} = r \left[ \cos\phi \sin\theta \, \bar{x} + \sin\phi \sin\theta \, \bar{y} + \cos\theta \bar{z} \right]$$

$$\bar{\rho}_3 = \bar{\rho} - \bar{\varepsilon}$$

where

$$\bar{\varepsilon} = \varepsilon_x \bar{x} + \varepsilon_y \bar{y} + \varepsilon_z \bar{z}$$

Hence

$$\bar{\rho}_3 = ( r \sin\theta \cos\phi - \varepsilon_x ) \bar{x} + ( r \sin\theta \sin\phi - \varepsilon_y ) \bar{y} + ( r \cos\theta - \varepsilon_z ) \bar{z}$$

$$r_3 = r \left[ (\sin\theta \cos\phi - \frac{\varepsilon_x}{r})^2 + (\sin\theta \sin\phi - \frac{\varepsilon_y}{r})^2 + (\cos\theta - \frac{\varepsilon_z}{r})^2 \right]^{\frac{1}{2}}$$

Where $r_3$ is the magnitude of $\bar{\rho}_3$.

For small feed displacements with respect to the focal point $\frac{\varepsilon_x}{r} << 1$ similarly for $\frac{\varepsilon_y}{r}$ and $\frac{\varepsilon_z}{r}$. Neglecting terms higher than the first order of these parameters, we get;

$$r_3 = r \left\{ 1 - \frac{2}{r} \left[ \sin\theta \left( \varepsilon_x \cos\phi + \varepsilon_y \sin\phi \right) + \cos\theta \, \varepsilon_z \right] \right\}$$

let $\varepsilon_t = \left[ \varepsilon_x^2 + \varepsilon_y^2 \right]^{\frac{1}{2}}$

and $\tan\phi_0 = \frac{\varepsilon_x}{\varepsilon_y}$

$$r = r \left\{ 1 - \frac{2}{r} \left[ \sin\theta \, \varepsilon_t \cos ( \phi - \phi_0 ) + \varepsilon_z \cos\theta \right] \right\}^{\frac{1}{2}}$$

Applying the binomial theorem and again neglecting terms higher than the first order in $\frac{\varepsilon}{r}$ and $\frac{\varepsilon}{r}$ we get;

$$r_3 = r \left[ 1 - \varepsilon_t \sin\theta \cos(\phi - \phi_0) - \varepsilon_z \cos\theta \right]$$

as the compensating phase term S is given by ;

$$S = r - r_3$$

Hence

$$S = \varepsilon_t \sin\theta \cos(\phi - \phi_0) + \varepsilon_z \cos\theta$$

To simplify the phase term $r - \overline{\rho} \cdot \overline{R_1}$

$$r - \overline{\rho}.\ \overline{R_1} = r - r\cos\Psi(\cos\theta\cos\theta_0 - \sin\theta\cos\phi\sin\theta_0) -$$
$$r\sin\Psi(\sin\theta\cos\phi\cos\Phi\cos\theta_0 + \cos\theta\cos\Phi\sin\theta_0 +$$
$$\sin\theta\sin\phi\sin\Phi$$

For small change of $\Psi$ around $180^0$ $\cos\Psi \simeq -1$ we get;

$$r - r\cos\Psi(\cos\theta\cos\theta_0 - \sin\theta\cos\phi\sin\theta_0) \simeq 2f$$

Hence, the exponential term will be reduced to;

$$-r\sin\Psi(\sin\theta\cos\phi\cos\Phi\cos\theta_0 + \cos\theta\cos\Phi\sin\theta_0 +$$
$$\sin\theta\sin\phi\sin\Phi) - S$$

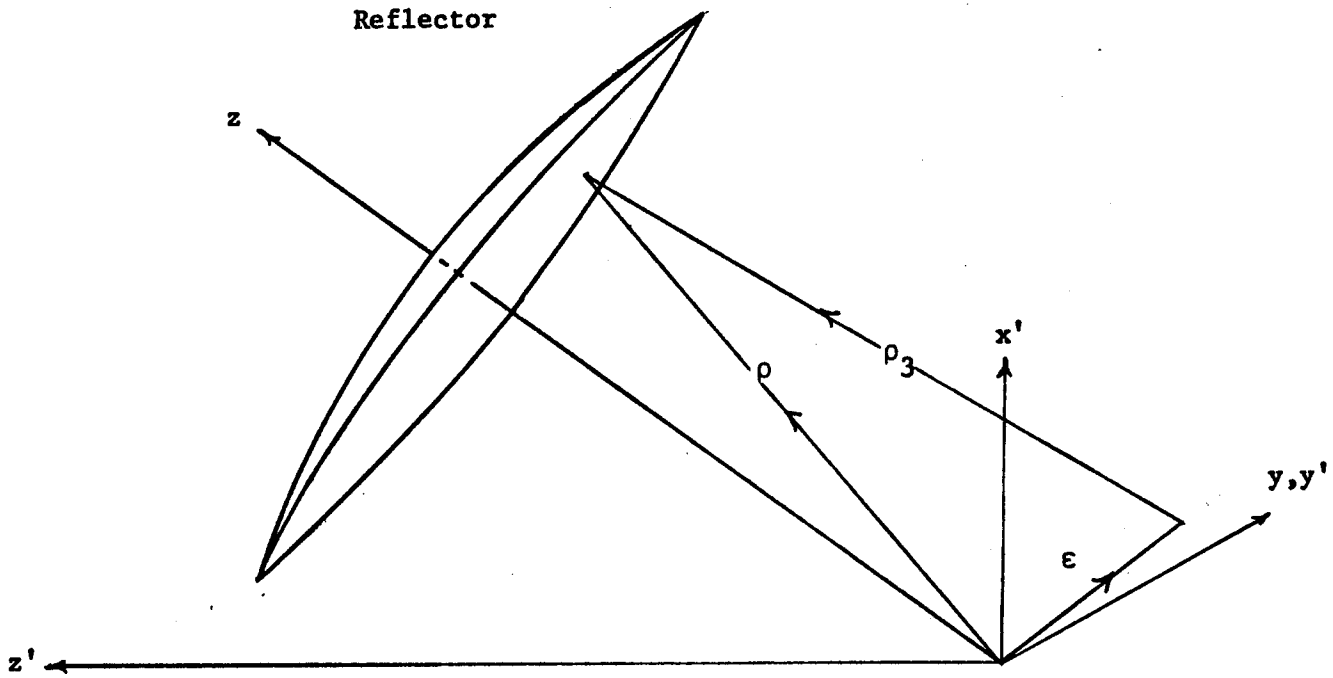


Figure 21. On The Phase Term Approximation

## Appendix C

## EQUATIONS GOVERNING THE RELATION BETWEEN THE X', Y', Z' AND THE $X_3, Y_3, Z_3$ AXES

The axis $x', y', z'$ are shifted by $\varepsilon_x$, $\varepsilon_y$, $\varepsilon_z$ respectively, as seen from figure (22.a) .

$$x_1 = x' - \varepsilon_x$$
$$y_1 = y' - \varepsilon_y$$
$$z_1 = z' - \varepsilon_z$$

The $z_1 y_1$ plane is now rotated by an angle $\eta$ so that the $x_2 z_2$ plane will pass by the vertex of the paraboloid, as seen from figure (22.b)

where

$$\tan\eta = \frac{\varepsilon_y}{R \cos\theta_0 - \varepsilon_z}$$

and

$$R = \frac{2f}{1 + \cos\theta_0}$$

Then the $x_2 z_2$ plane is rotated by an angle $\Psi_0$ such that the $z_3$ axis will pass thorough the vertex of the paraboloid, as seen from figure (22.c)

$$\tan \Psi_0 = \frac{R \sin\theta_0 - \varepsilon_x}{\sin\eta\, \varepsilon_y + \cos\eta\, ( R \cos\theta_0 - \varepsilon_z )}$$

And the relation between the $x_3, y_3, z_3$ and the $x', y', z'$ coordinate systems can be represented in the matrix form as follows;

$$\begin{bmatrix} x_3 \\ y_3 \\ z_3 \end{bmatrix} = \begin{bmatrix} \cos\Psi_0 & \sin\Psi_0 \sin\eta & -\sin\Psi_0 \cos\eta \\ 0 & \cos\eta & \sin\eta \\ \sin\Psi_0 & -\cos\Psi_0 \sin\eta & \cos\Psi_0 \cos\eta \end{bmatrix} \begin{bmatrix} x' \\ y' \\ z' \end{bmatrix} \quad (1)$$

With reference to figure ( 21), the relation between the spherical coordinates is driven as follows;

$$\bar{\rho}_3 = \bar{\rho} - \bar{\varepsilon}$$

$$\bar{\varepsilon} = \varepsilon_x \bar{x}' + \varepsilon_y \bar{y}' + \varepsilon_z \bar{z}'$$

$$\bar{\rho} = r ( \sin\theta' \cos\phi' \bar{x}' + \sin\theta' \sin\phi' \bar{y}' + \cos\theta' \bar{z}' )$$

$$\bar{\rho}_3 = r_3 ( \sin\theta \cos\phi \bar{x}_3 + \sin\theta \sin\phi \bar{y}_3 + \cos\theta \bar{z}_3 ) \quad (2)$$

Hence

$$\bar{\rho}_3 = ( r \sin\theta' \cos\phi' - \varepsilon_x ) \bar{x}' + ( r \sin\theta' \sin\phi' - \varepsilon_y ) \bar{y}'$$
$$( r \cos\theta' - \varepsilon_z ) \bar{z}'$$

substituting the values of x',y',z' from equation ( 1 ) we get;

$$\begin{aligned}\bar{\rho}_3 = \{ &( r\sin\theta'\cos\phi' - \varepsilon_x )\cos\Psi_0 + (r\sin\theta'\sin\phi' - \varepsilon_y) \\ &(\sin\Psi_0\sin\eta ) + ( r\cos\theta' - \varepsilon_z ) ( -\sin\Psi_0\cos\eta ) \} \bar{x}_3 + \\ \{ &( r\sin\theta'\sin\phi' - \varepsilon_y )\cos\eta + ( r\cos\theta' - \varepsilon_z )\sin\eta \} \bar{y}_3 + \\ \{ &( r\sin\theta'\cos\phi' - \varepsilon_x )\sin\ + ( r\sin\theta'\sin\theta' - \varepsilon_y ) \\ &(-\cos\Psi_0\sin\eta ) + ( r\cos\theta' - \varepsilon_z )\} \bar{z}_3 \end{aligned} \qquad (3)$$

By equating the coefficients of $x_3, y_3, z_3$ in (2) and (3) we finally get

$$\begin{aligned} r_3\sin\theta_3\cos\phi_3 &= ( r\sin\theta'\cos\phi' - \varepsilon_x )\cos\Psi_0 + \\ &\quad (r\sin\theta'\sin\phi' - \varepsilon_y )\sin\Psi_0\sin\eta - \\ &\quad (r\cos\theta' - \varepsilon_z )\sin\Psi_0\cos\eta \\ r_3\sin\theta_3\sin\phi_3 &= ( r\sin\theta'\sin\phi' - \varepsilon_y )\cos\eta + \\ &\quad ( r\cos\theta' - \varepsilon_z )\sin\eta \\ r_3\cos\theta_3 &= ( r\sin\theta'\cos\phi' - \varepsilon_x )\sin\Psi_0 - \\ &\quad ( r\sin\theta'\sin\theta' - \varepsilon_y )\cos\Psi_0\sin\eta + \\ &\quad ( r\cos\theta' - \varepsilon_z )\cos\Psi_0\cos\eta \end{aligned}$$

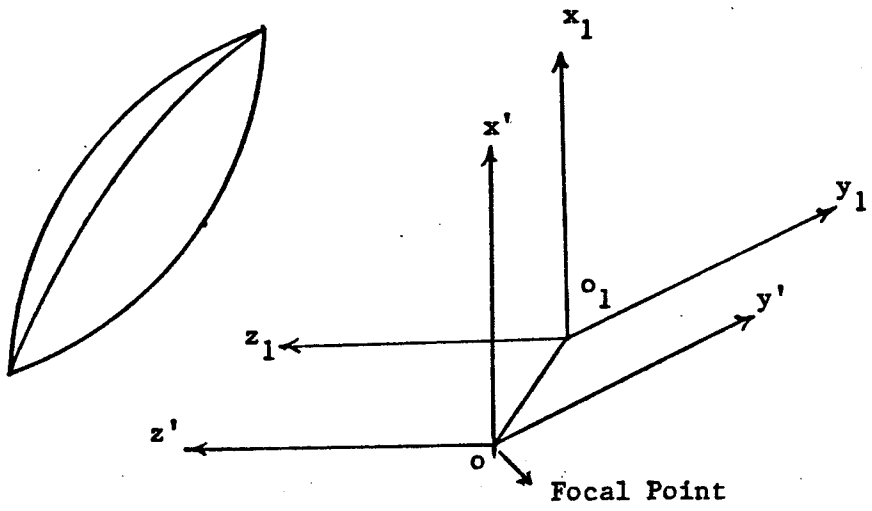


a. The Shift of The Axes From o' to $o_1$

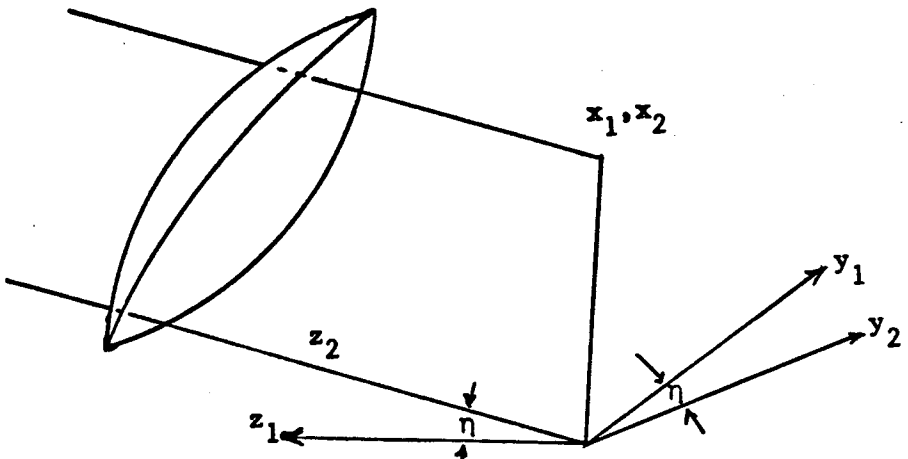


b. The Rotation of The $z_1y_1$ Plane to $z_2y_2$ Plane Such That The $z_2x_2$ Plane Becomes The Reflector Plane of Symmetry

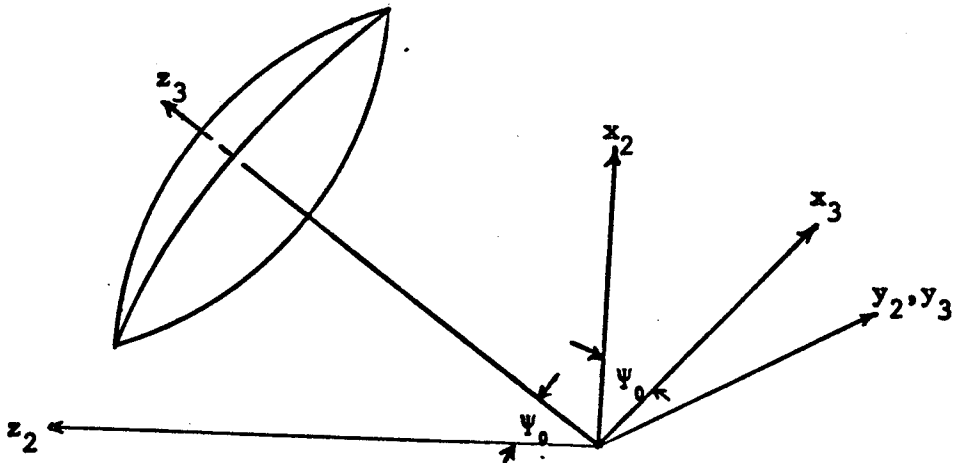


c. The Rotation of The $z_2x_2$ Plane, So That, $z_3$ Becomes The Reflector Axis of Symmetry

Figure22. The Shift and The Rotation of The Axes

## REFERENCES


[1] Chugh R.K "Dielectric Cone and Reflecting Antennas" Ph.D. Thesis. University of Manitoba. 1977

[2] Cutler C.C "Parabolic Antenna design for Microwaves" Proc. IRE, 35 (11), pp 1284-1294, Nov. 1947.

[3] Love, A.W., "Some Highlights in Reflector Antenna Development" Radio sci., vol.11, pp. 671-684, 1976.

[4] Galindo, V., "Design of Dual Reflector Antennas with Arbitrary Phase and Amplitude Distribution," IEEE trans. Antenna Propagt. AP.(12), pp. 403-408, 1963.

[5] Williams, W.F., "High Efficiency Antenna Reflectors," Microwave J. 8(7), pp. 79-82, 1965.

[6] Potter, P.D. and Ludwig, A.C., "Beam Shaping by use of Higher Order Modes in Conical Hornes," NEREM Record 1963, Vol, pp. 92-95 .

[7] Ruze, J., "Lateral Feed Displacement in a Paraboloid," IEEE trans. Antenna Propagat. Vol. 13, pp. 660-665, Sept. 1965.

[8] Imbrial, W.A. and Ingerson, P.G. and Wong, W.C., "Large Lateral Feed Displacement in a Parabolic Reflector," IEEE trans. Antenna Propagat. Vol AP 22, pp. 742-745, nov. 1974.

[9] Shafai, L. and Zaghloul, A.A., "Performance of offset Paraboloid Reflector Antennas with Offset Matched Feeds," DSS file No. OST78-00024 final report, March 1979.

[10] Cook, J.S. and Elamand, E.M. and Zucker, H., "The Open Cassegrian Antenna- Part 1: Electromagnetic Design and Analyses," Bell syst. tech.J., Vol.44, pp. 1255-1300, 1965.

[11] Chu, T.S. and Turrin, R.H., "Depolarization Properties of Offset Reflector Antennas," IEEE trans. Antenna Propgat. Vol. AP-21, pp. 339 345, May 1973.

[12] Rudge, A.W., "Multiple-Beam Antennas: Offset Reflectors with Offset Feeds," IEEE trans. Antenna Propagat. Vol. AP.23, pp. 317-322, may 1975. in

[13] Jacobsen, J., "On the Cross Polarization of Asymmetric Reflector Antennas for Satelitte Applications," IEEE trans. Antenna Propagat., Vol AP-25, pp. 276-283, March 1977.

[14] Rudge, A.W. and Adatia, N.A., "New Class of Primary Feed Antennas for Use with Offset Parabolic Reflector Antennas," Electronic Letters, Vol.11, No.24, pp. 597-599, Nov. 1975.

[15] Aboul-Atta, O. and Shafai, L., "Vector Radiation Pattern for Offset Prime Focus Paraboloid Antennas Illuminated by Matched Primary Feeds," Department of Electrical Engineering, University of Manitoba. EE-TR-78-01.

[16] Minnet, H.C., "A Method of Synthesizing Radiation Pattens with Axial Symmetry," IRE trans. Antenna Propagat. AP-2, pp. 119-127, sept. 1966.

[17] Bem, D.J., "Electric Field Distribution in the Focal Region of an Offset Paraboloid," Proc.IEE, Vol.116, No.5, pp. 679-684, 1969.

[18] Vallintino, A.R. and Toulios, P.P., "Fields in the Focal Region of Offset Parabolic Antennas," IEEE trans. Antenna Propagat. pp. 859-865, nov. 1976.

[19] Ludwig, A.C., "The Definition of Cross Polarization," IEEE trans. Antenna Propagat. Vol. AP-21, pp. 116-119, jan. 1973.

[20] "IEEE Standard Definitions of Terms for Antennas," IEEE trans. Antenna Propagat. Vol. AP-17, pp. 262-269, may 1969.

[21] Rudge, A.W. and Adatia, N.A., "Offset Parabolic Reflector Antennas: A Review" Proc IEEE, Vol.66, No.12, pp. 1592-1618, dec. 1978.

[22] Silver, S., "Microwave Antenna Theory and Design" New York: Mc Graw-Hill, 1949.

[23] Tsai, L.L., "A Comparison of GTD and IEF for Analysis of Reflector Antennas" IEEE trans. Antenna Propagat., Vol. AP-20, pp. 705-712, nov. 1972.

[24] Chugh, R.K. and Shafai, L., "Comparison of Integration Algorithms for the Evaluation of Rapidly Varying Integrals," Large Engineering systems, Editor A.Wexler, Pergamon press.

[25] Lessow, H.A., Rusch, V.T., and Jacobsen, H.S., "On Numerical Evaluation of two Dimensional Phase Integrals," IEEE trans. Antenna Propagat. Vol. AP-23, pp. 714-717, sept. 1975.

[26] Lo, Y.T., "On the Beam Deviation Factor of a Parabolic Reflector," IRE trans. Antenna Propagat. Vol. AP-8, pp. 347-349, may 1960.